# Supporting Information

# Tuning Between Quenching and Energy Transfer in DNA-Templated Heterodimer Aggregates

*Azhad U. Chowdhury,[†] Sebastián A. Díaz,[‖] Jonathan S. Huff,[†] Matthew S. Barclay,[†] Matthew Chiriboga,[‖,^] Gregory A. Ellis,[‖] Divita Mathur,[‖,θ] Lance K. Patten,[†] Aaron Sup,[‡] Natalya Hallstrom,[†] Paul D. Cunningham,[Π] Jeunghoon Lee,[†,§] Paul H. Davis,[†] Daniel B. Turner,[†] Bernard Yurke,[†,§] William B. Knowlton,[†,§] Igor L. Medintz,[‖] Joseph S. Melinger, [Π] and Ryan D. Pensack[†,*]*

[†]Micron School of Materials Science & Engineering, [‡]Department of Physics, [§]Department of Chemistry & Biochemistry, and [§]Department of Electrical & Computer Engineering, Boise State University, Boise, Idaho 83725, United States

[‖]Center for Bio/Molecular Science and Engineering Code 6900, [Π]Electronics Science and Technology Division Code 6800, U.S. Naval Research Laboratory, Washington, D.C. 20375, United States

[^]Volgenau School of Engineering, George Mason University, Fairfax, VA 22030, United States

[θ]College of Science, George Mason University, Fairfax, VA 22030, United States

Table of Contents:

## Section S1. Chemical structures of Cy5 and Cy5.5

**Figure S1** displays the chemical structures of Cy5 and Cy5.5. The two benzene rings in Cy5.5 increase the π-conjugation, which results in distinct optical properties compared with Cy5 and thus optical selectivity between the two dyes.

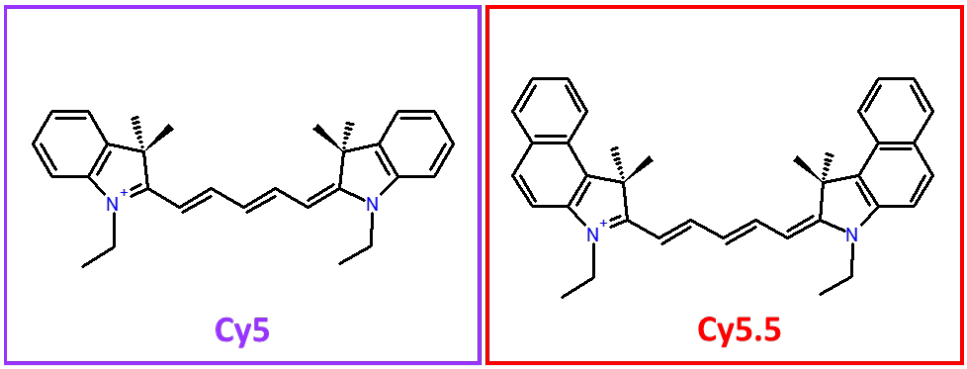


**Scheme S1.** Chemical structures of Cy5 and Cy5.5.

**Section S2. Synthesis of Cy5 and Cy5.5 labeled oligonucleotides and assembly of DNA Holliday junction constructs**

*Synthesis of Cy5 and Cy5.5 labeled oligonucleotides*

Cy5 labeled oligonucleotides were synthesized according to the sequences of Cannon *et al.*,[1] see e.g. **Table S2**.

**Table S2.** Oligonucleotide Sequences

| Strand Name | Sequence (5' to 3') | Length (nt) | Purification |
|---|---|---|---|
| **A** | ATATAATCGCTCGCATATTATGACTG | 26 | Standard Desalting |
| **B** | CAGTCATAATATGTGGAATGTGAGTG | 26 | Standard Desalting |
| **C** | CACTCACATTCCACTCAACACCACAA | 26 | Standard Desalting |
| **D** | TTGTGGTGTTGAGCGAGCGATTATAT | 26 | Standard Desalting |
| **Cy5-A** | ATATAATCGCTCG/iCy5/CATATTATGACTG | 26 | HPLC |
| **Cy5.5-B** | CAGTCATAATATG/iCy5.5/TGGAATGTGAGTG | 26 | HPLC |
| **Cy5.5-C** | CACTCACATTCCA/iCy5.5/CTCAACACCACAA | 26 | HPLC |

Briefly, solid phase phosphoramidite coupling chemistry was carried out at 1 µM scale with controlled pore glass columns using an Expedite 8909 Applied Biosystems Expedite 8909 DNA Oligo Synthesizer. Coupling time for the Cy5 phosphoramidite was set at 6 minutes. 4-6 copies of each target oligonucleotide were synthesized. All DNA and dye phosphoramidite precursors along with the synthetic reagents were obtained from Glen Research. Synthesized oligonucleotides were deprotected using 7.5% ammonium hydroxide overnight at room temperature followed by desalting using a C18 reverse phase media disposable column and 0.2 M triethylammonium acetate buffer. The sequence and presence of the correct oligonucleotide was confirmed using a SQD2, a single quadrupole mass spectrometer which was coupled to a Waters Acquity H-Class UPLC for LC-MS with an ESI source. System control and data acquisition was achieved with MassLynx V4.1 software.[2] The *m*/*z* of the Cy5-labeled oligonucleotide was found to be within ≤ 1 *m*/*z* unit difference from that predicted (**Figure S2.1**). Oligos were purified to >95% using a Waters Prep LC 150 preparatory system, aliquoted, and dried down for storage at -20 °C in the dark until needed when they were resolubilized as described.

Cy5.5 containing oligonucleotides (**Table S2**) were obtained from Integrated DNA Technologies IDT at 1 µM scale synthesis. The *m*/*z* of all Cy5.5-labeled oligonucleotides was found to be within ≤ 1 *m*/*z* unit difference from that predicted (**Figures S2.2 and S2.3**).

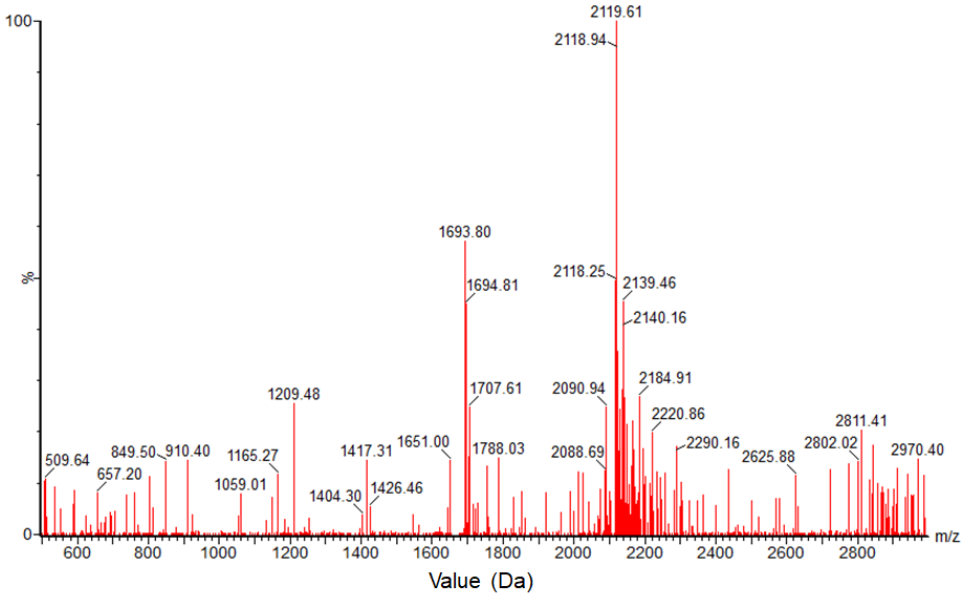


**Figure S2.1.** Mass spectrum for the Cy5-A strand (sequence shown in **Table S2**). The predicted *m*/*z* was 1694.12 (*z* = 5) and 2117.90 (*z* = 4); the measured *m*/*z* was 1693.77 (*z* = 5) and 2118.94 (*z* = 4).

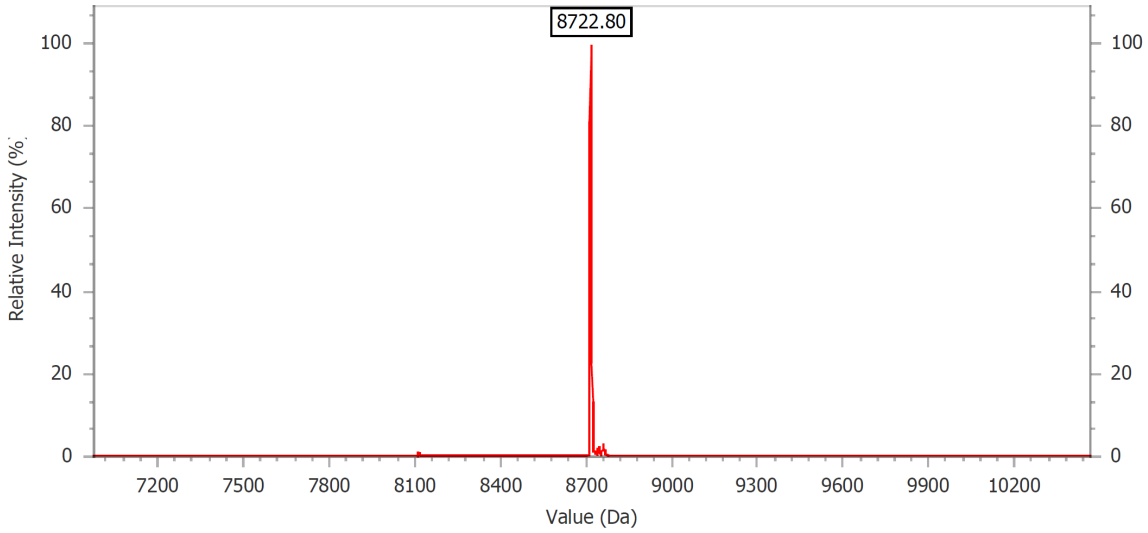


**Figure S2.2.** Mass spectrum for the Cy5.5-B strand (obtained from Integrated DNA Technologies). The Cy5.5-B sequence is shown in **Table S2**. The predicted *m*/*z* was 8722.0; the measured *m*/*z* was 8722.8.

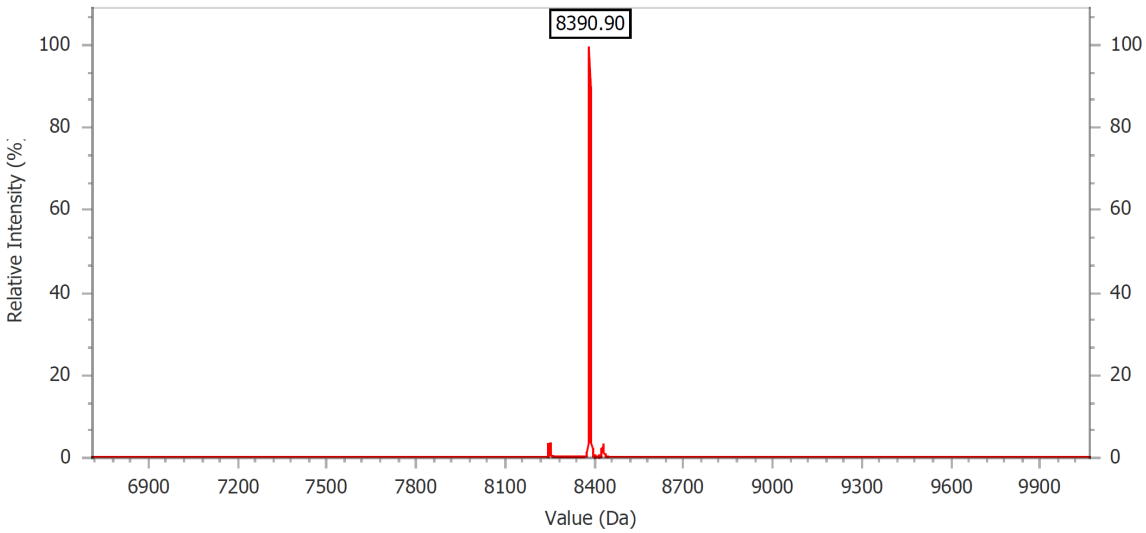


**Figure S2.3.** Mass spectrum for the Cy5.5-C strand (obtained from Integrated DNA Technologies). The Cy5.5-B sequence is shown in **Table S2.** The predicted *m*/*z* was 8389.9; the measured *m*/*z* was 8390.9.

*Assembly of DNA Holliday junction dye constructs*

The Cy5/Cy5.5 dye-labeled and corresponding non-dye-functionalized strands were rehydrated with ultrapure water (Barnstead Nanopure, Thermo Scientific) to produce a 100 µM stock solution. DNA four-armed junctions were prepared by combining equimolar amounts of the complementary oligomers that assembled into a given target structure in a 1 × TAE (40 mM tris-(hydroxymethyl) aminomethane, 20 mM acetic acid, 1 mM ethylenediaminetetraacetic acid) buffer solution (pH 8.0) with 15 mM added magnesium chloride ($MgCl_2$) to obtain a final DNA concentration of 10 µM in 100 uL. Samples in 0.5 mL PCR tubes underwent annealing/hybridization overnight in an Eppendorf Mastercycler using the following program: Lid temperature = 95˚C constant; Step 1 T = 95˚C for 5 minutes; Step 2 T = 94˚C to 85˚C for 5 minutes/1˚C drop; Step 3 T = 85˚C for 10 minutes; Step 4 T = 84˚C to 4˚C for 10 minutes/1˚C drop; Step 5 T = 4˚C till samples were removed for experiments or storage in the refrigerator. TAE buffer (10 × stock solution, pH 8.0) and $MgCl_2$ (99% purity) were purchased from Fisher Scientific. Assembly of DNA four-armed junctions was confirmed by gel electrophoresis (**Figures S2.4 and S2.5**).

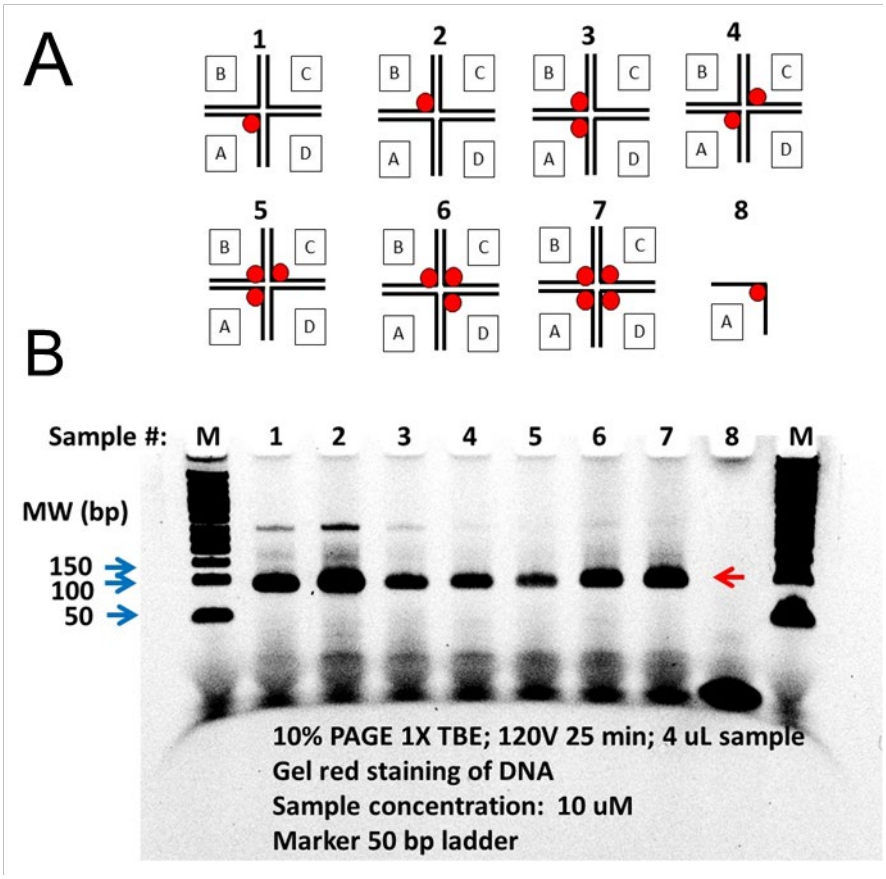


**Figure S2.4. Polyacrylamide gel electrophoresis analysis of different dye combinations in four-armed junction structures.** (**A**) A series of samples were assembled with different dye combinations present to evaluate four-armed junction formation efficiency. (**B**) Following hybridization as described, the samples were separated in 10% polyacrylamide gels and stained with gel red to visualize their structures. The gel image shows that all structures were formed with ≥ 95% efficiency (red arrow) and they were therefore used as is. Some small higher molecular weight bands do appear in some lanes (<5%) which we ascribe to higher molecular weight concatemers. Critically, there does not appear to be any substantial staining below the main product band which would correspond to partially formed structures.

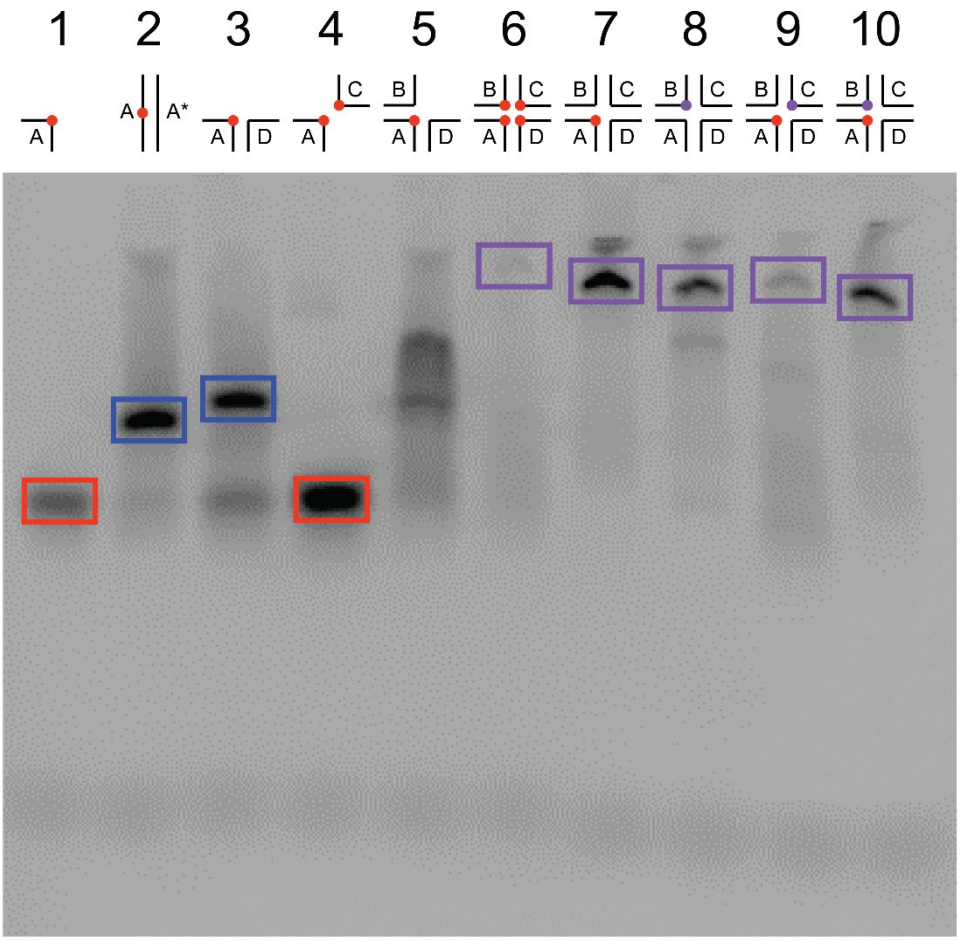


**Figure S2.5. Polyacrylamide gel electrophoresis measurements of dye labeled single-stranded (ss) DNA, double-stranded (ds) DNA, DNA Holliday junction (HJ) fragments, and DNA HJs.** The samples were separated in 15% polyacrylamide gel. The lane numbers are indicated above the image along with the sample placed in each lane. Various forms of dye labeled ss DNA, ds DNA, DNA HJ fragments, and DNA HJs (labeled according to Cannon *et al.*[1] [lanes 1-7] and **Table S2** [lanes 7-10]) were used. Black lines represent oligonucleotides and Cy5 and Cy5.5 dyes are represented by red and purple circles, respectively. The images were obtained by exciting the gel at 645 nm and detecting the DNA with a Cy5 dye filter at 648-668 nm. Lane 1 depicts the lowest band, highlighted with a red square, which consists of ss DNA Cy5 monomer A. Lane 4 migrates at the same rate as lane 1, indicating that Cy5-labeled A and Cy5-labeled C cannot hybridize as expected. Lanes 2 and 3 show that Cy5-labeled A can hybridize with its complementary Cy5-labeled strand along with Cy5-labeled D, as is evident in the bands highlighted with blue squares. The most intense bands of lane 5, which consists of a HJ fragment, are situated below the most intense bands in lanes 6-10. The sample in lane 6 is a DNA-Holliday junction templated Cy5 tetramer reference control, according to Cannon *et al.*[1] The observation is strong evidence that the most intense bands in lanes 6-10, highlighted with purple squares, arise from four-armed DNA HJs. Note that the bands in lanes 6 and 9 are faint due to fluorescence quenching.

## Section S3. Optical spectroscopy experimental methods

### *S3.1. Steady state spectroscopy*

#### *S3.1.1. UV-VIS absorption*

Absorption spectra were measured using a Cary 60 UV-Vis spectrophotometer (Agilent Technologies; Santa Clara, CA, USA) for all samples. Measurements were performed within the spectral range of 200-800 nm, with 1 nm step intervals and a 0.1 second integration time. Sample solutions were prepared at a concentration of 2 μM and measurements were made in a 2 mm path length quartz spectrophotometer cell (Starna Cells, Inc.; Atascadero, CA, USA).

#### *S3.1.2. Circular dichroism*

Circular dichroism measurements (CD) were performed using a JASCO J-1500 CD spectrophotometer. The samples were placed in a 10 mm pathlength quartz cuvette (150 μL volume) at a concentration of 2 μM of DNA structure, within the spectral range of 200-800 nm, with 1 nm step intervals, 200 nm/min, 2 s digital integration time, at 20 °C.

#### *S3.1.3. Fluorescence emission*

Fluorescence emission was measured using a TECAN plate reader exciting from above. An excitation wavelength of 615 nm was used to excite the sample and the fluorescence emission was measured from 630-900 nm with 1 nm steps. 100 μl of a 1 μM solution was added to a 96 well black plate, resulting in a 1.25 mm pathlength and a maximum OD of 0.05 avoiding inner filter effects.

#### *S3.1.4. Fluorescence quantum yield*

Relative fluorescence quantum yield (FQY) measurements were performed on a Fluoromax-3 spectrofluorometer (Horiba Scientific). Typical scan parameters of 615 nm excitation wavelength, 1 nm steps, 0.5 s integration time and fixed slit width were used for all samples. A solution was prepared by diluting each sample in 1× TAE in 15 mM $MgCl_2$ buffer and transferred into a 3 mm quartz cuvette for all measurements. Samples were measured at multiple dilutions, with OD ≤ 0.1 at 615 nm (excitation wavelength). The slopes of each sample were compared to the slope of both Rhodamine 800 (FQY = 0.247 ± 0.030)[3] and Oxazine 720 (FQY = 0.63 ± 0.05)[4]. Values were very similar (though oxazine was always slightly higher than the rhodamine value) and the final reported value is the average of the two. Uncertainties are propagated from the uncertainties of the standards, uncertainty of the slope fit, and the averaging of the values.

### *S3.2. Transient absorption spectroscopy*

Transient absorption measurements in the visible and near-infrared spectral regions were performed with a 1 kHz regeneratively amplified Ti:sapphire laser system (Coherent Astrella, Santa Clara, California) that delivers ~100 fs pulses at ~800 nm with an average power of ~6 W. A beamsplitter at the output of the laser amplifier served to generate separate pump and probe beam paths. ~2 W of the output power was used to drive an optical parametric amplifier (Light Conversion OPerA Solo, Vilnius, Lithuania) to convert the 800 nm radiation to pump wavelengths

of 615, 650 and 690 nm (**Figure S3.2.1**). The pump pulse duration was measured to be ~230 fs for the pump wavelength of 650 nm (**Figure S3.2.2)**. The pump and a small fraction of the power of the laser amplifier were directed into the TA spectrometer. The 800 nm light was used to generate a continuum in either the visible (ca. 420 to 760 nm) or near-infrared (ca. 820 to 1600 nm) spectral region (**Figure S3.2.3**). Optical filters were used to isolate the continuum from the 800 nm fundamental light. The pump polarization was controlled by a Glan-Thompson linear polarizer (Newport Corporation, Irvine, CA) and an achromatic λ/2 waveplate (Tower Optical Corporation, Boynton Beach, Florida), and the probe polarization was controlled with a Glan-Laser polarizer (Thorlabs Inc., Newton, New Jersey) in the probe beam path situated before continuum generation. Measurements were performed with pump and probe polarizations oriented at the magic angle at the sample.

The samples (5 μM dye constructs in 1× TAE in 15 mM $MgCl_2$ buffer) were contained in a 2 mm path length quartz spectrophotometer cell (Starna Cells, Inc., Atascadero, California) for the transient absorption measurements. The optical density of the samples varied from ca. 0.04 to 0.32 at the excitation wavelength. The beam spot size for pump wavelengths of 615, 650 and 690 nm was estimated to be 109, 114 and 123 μm, respectively, by using an sCMOS camera (Thorlabs, Newton, New Jersey) situated at the focal plane of the probe beam. The pump power was measured with a high-sensitivity optical power sensor (Coherent, Santa Clara, California). Incident pump fluences in the visible and near-infrared spectral regions were ≤30 and ≤80 $\mu J/cm^2$, respectively. The sample was stirred during all measurements using a magnetic bar in the spectrometer cell rotated by a magnetic stirrer (Ultrafast Systems Helios, Sarasota, Florida). In order to achieve high signal-to-noise ratios necessary for global analysis, between 25 and 256 scans were acquired and averaged depending on the signal amplitude in the femtosecond visible and near-infrared transient absorption measurements. To suppress baseline signals, including static pump scatter, a negative time delay spectrum, averaged over multiple negative time delays, was subtracted from the entire dataset.

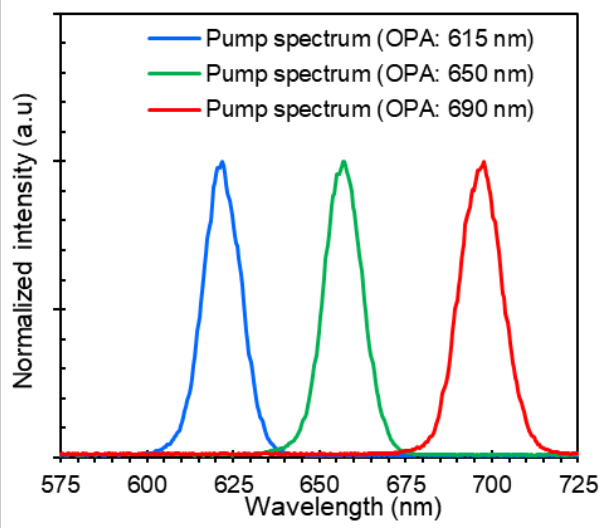


**Figure S3.2.1**. Representative spectra of the three different pump beams (i.e., 615, 650 and 690 nm) used in transient visible and near-infrared absorption measurements.

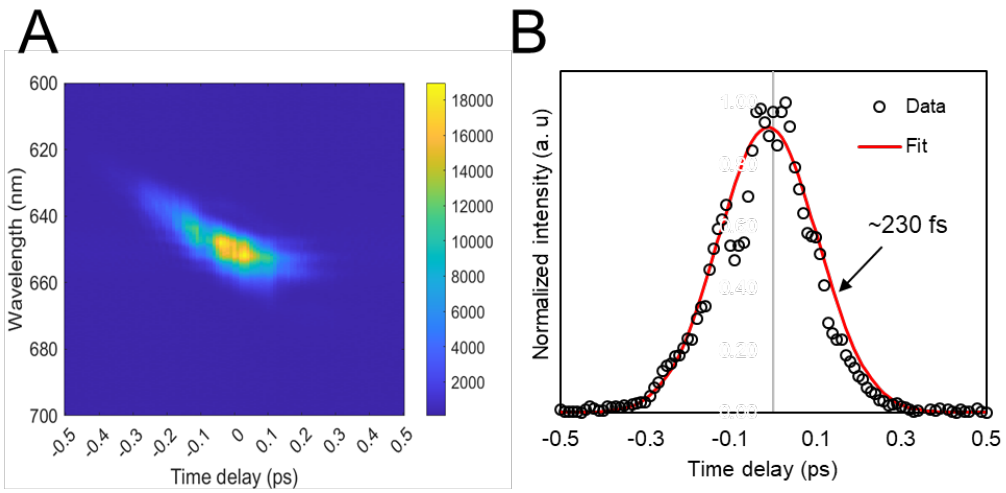


**Figure S3.2.2.** Transient-grating frequency-resolved optical gating (TG-FROG) characterization[5] of 650 pump beam. The beam was taken before the transient absorption spectrometer and a comparable amount of glass was added to the beam path to compensate for the amount of glass in the transient absorption spectrometer. The TG FROG signal was generated in a 1 mm thick Infrasil (Thorlabs, Newton, New Jersey). (**A**) TG-FROG surface plot. (**B**) Spectrally-integrated time trace along with Gaussian fit indicating a pulse duration of ~230 fs.

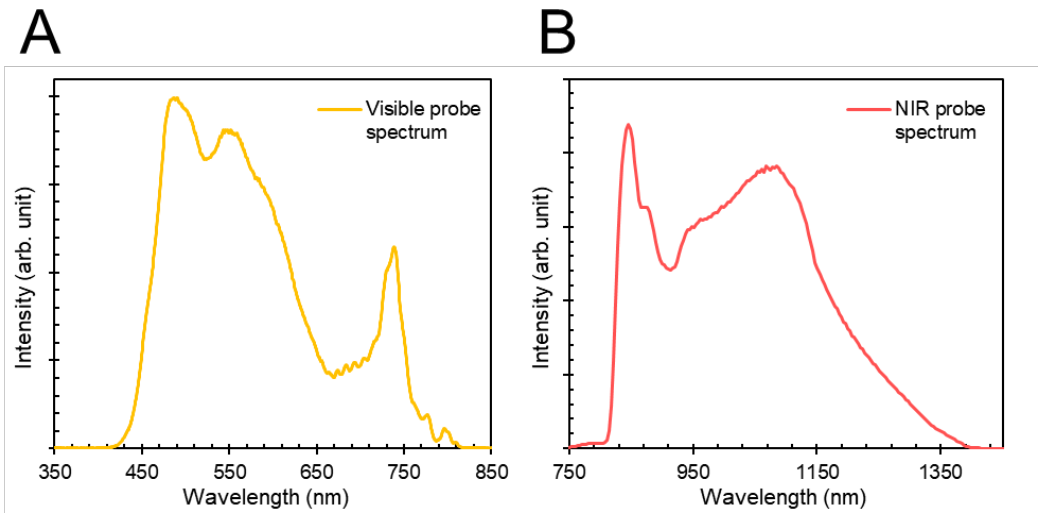


**Figure S3.2.3.** Representative spectra of visible (A) and near-infrared (B) probe beams used in transient visible and near-infrared absorption measurements, respectively.

## Section S4. Theoretical modeling methods

The optical properties (absorption and circular dichroism spectra) of transverse heterodimer along with Cy5 and Cy5.5 transverse homodimers were modeled with an approach based on Kühn−Renger−May (KRM) theory.[6] KRM modeling was previously employed to obtain insight into the dye aggregate system such as dye separation distance, packing (relative orientation) and coupling strength, detail on KRM modeling described elsewhere.[1,7–9] Briefly, the excitonic hopping parameter, $J_{m,n}$, is related to the square of the TDMs and distance between them, but when the distance between dyes approaches the length of the dipoles a more accurate expression is required. Therefore, the extended dipole approximation was used in the modeling.

## Section S5. Extinction spectra of Cy5 and Cy5.5 monomer solutions

We measured the extinction ($\varepsilon$) spectra of Cy5 and Cy5.5 monomer solutions (**Figure S5)**. The peak wavelengths and peak extinction coefficients are listed in **Table S5**.

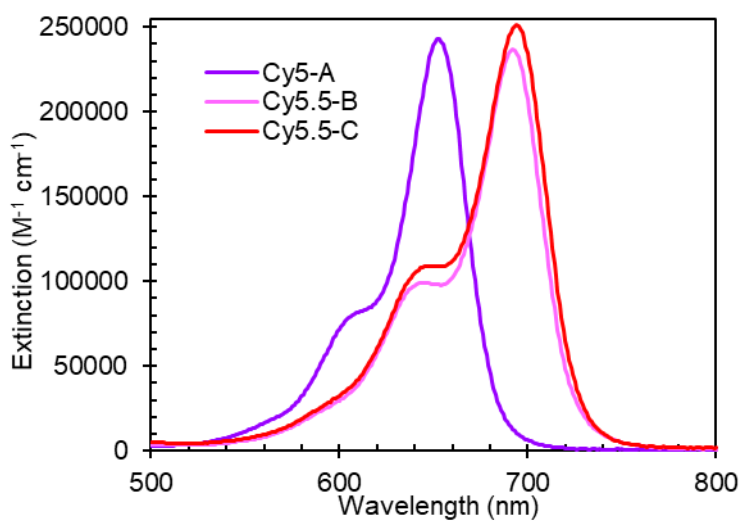


**Figure S5.** Extinction spectra of Cy5-A, Cy5.5-B and Cy5.5-C monomer solutions.

**Table S5**. Peak wavelengths and extinction coefficients of Cy5 and Cy5.5 monomer solutions.

| Structure | $\lambda_{\varepsilon,max}$(nm) | $\varepsilon_{max}$($M^{-1}cm^{-1}$) |
|---|---|---|
| $A_5$BCD | 653 | 243,000 |
| AB5.5CD | 694 | 237,000 |
| ABC5.5D | 695 | 251,000 |
| **Average** | | 244,000 |

The extinction of the dyes is related the transition dipole moment ($\mu$) amplitude.[10] Since the peak extinction coefficients of the monomers are very similar, $\mu$ is expected to be very similar. These peak extinction coefficients are also consistent with a fully allowed electronic transition, and so, a maximal $\mu$. Thus, because both the strength of excitonic interactions and the rate of energy transfer are expected to depend on the $\mu$, the monomers have the potential to exhibit strong excitonic interactions (see e.g. ref. [11]) and they also have the potential to undergo rapid energy transfer (see e.g. refs. [12–14]).

**Section S6. Circular dichroism spectroscopy of monomer and heterodimer solutions**

To further characterize the optical properties of the transverse and adjacent heterodimer solutions, we performed circular dichroism (CD) spectroscopic measurements. **Figure S6** displays the CD spectra of 5μM Cy5 monomer, Cy5.5 monomer, transverse heterodimer, and adjacent heterodimer solutions. Panels **A** and **B** show that the monomer solutions do not produce any detectable signal in the visible spectral region, while the dimer solutions (panel **C** and **D**) exhibit a combination of positive and negative signals in this region. The positive and negative signals present in the CD spectra of the dimer solutions are consistent with excitonic coupling between dyes. Therefore, both heterodimer solutions have structures where dyes are excitonically coupled.

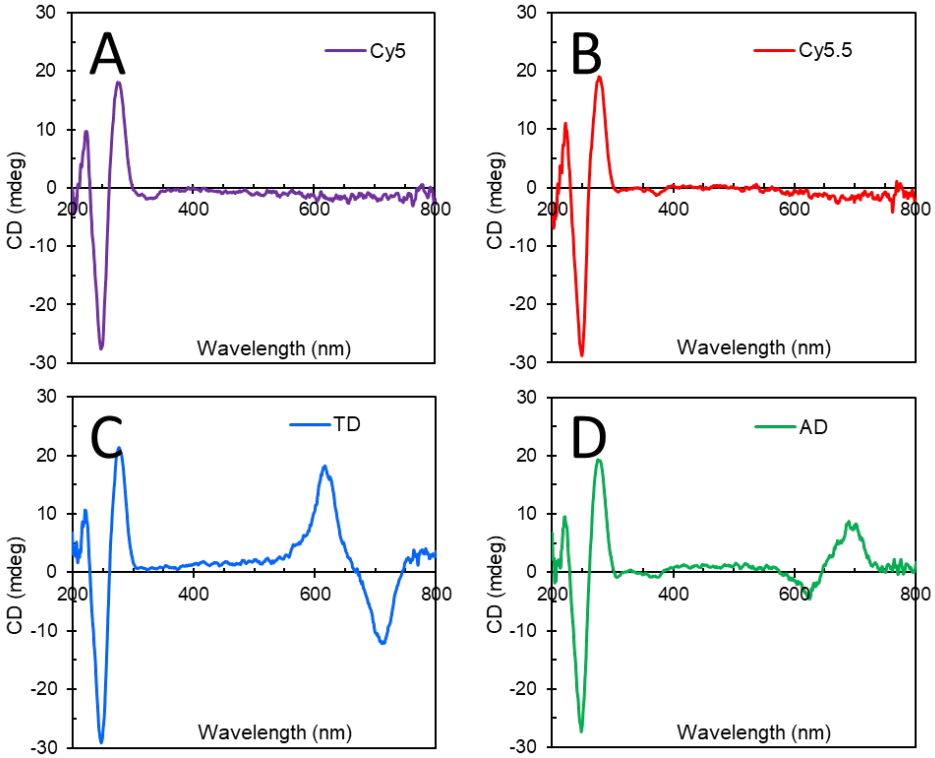


**Figure S6.** Circular dichroism spectra of Cy5 monomer, Cy5.5 monomer, transverse heterodimer, and adjacent heterodimer are presented in panels **A**, **B**, **C** and **D**, respectively. While the monomers do not produce any signal in the visible spectral region, the circular dichroism signal from transverse and adjacent heterodimer solution indicates an electronically coupled structure with different chirality that is present in both solutions.

**Section S7. Absorption and circular dichroism spectra of transverse and adjacent heterodimers from different spatial permutation of Cy5 and Cy5.5 at Holliday junction**

To investigate the DNA strand dependency on the optical properties of heterodimers, we studied a set of dimer samples in which the dyes are attached to different DNA strands at the Holliday junction. The results are presented in **Figure S7**. All transverse and adjacent dimers exhibit similar optical properties for both absorption and circular dichroism. Thus, the optical properties are largely independent of the spatial permutation of Cy5 and Cy5.5 at the Holliday junction. These results suggest that the DNA is bringing the dyes in close proximity and that the dye interactions are driving the dye-dye packing.

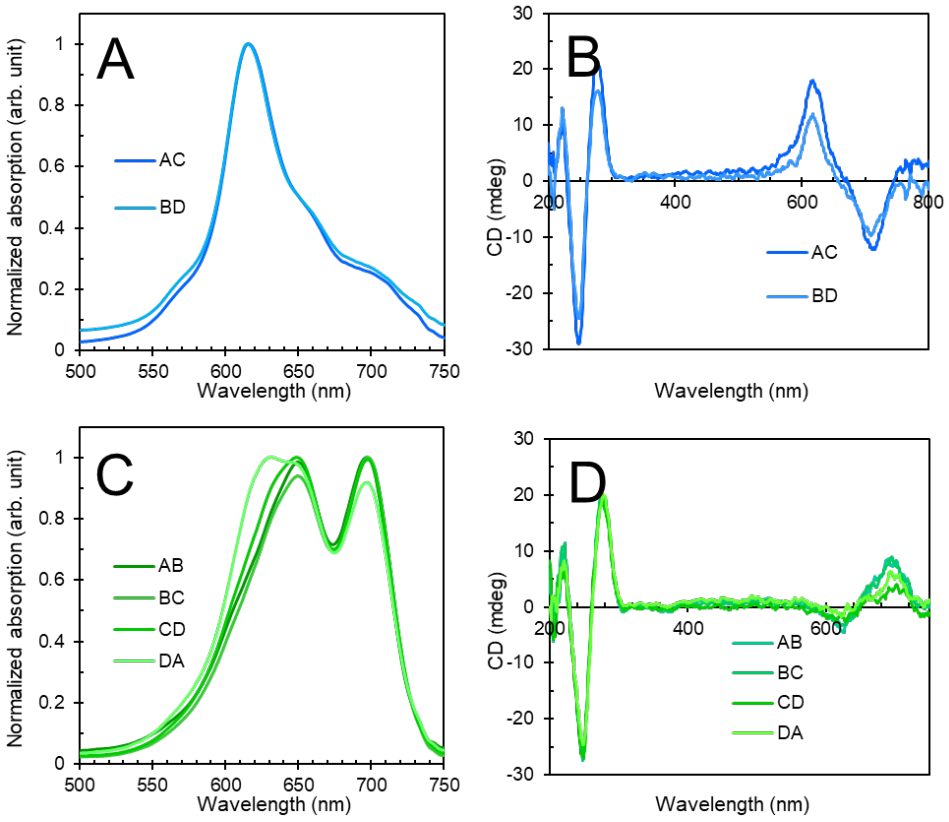


**Figure S7.** Panels **A** and **B** show the absorption and circular dichroism spectra of transverse heterodimer solutions (top row) and panels **C** and **D** show the absorption and circular dichroism spectra of adjacent heterodimers (bottom row). Letters in the legend in each figure represent the DNA strand where the dyes are attached to and Cy5.5 follows Cy5 in ordering. For example, AB means Cy5 is attached to DNA strand A and Cy5.5 to DNA strand B.

**Section S8. Absorption and circular dichroism spectra of transverse hetero- and homo-dimer solutions**

To further investigate the dye packing structure of the transverse heterodimer, the absorption and circular dichroism (CD) spectra of the transverse Cy5-Cy5.5 heterodimer solution is plotted along with Cy5 and Cy5.5 transverse homodimer solutions (**Figure S8**). The spectral features of the transverse heterodimer solution both in absorption and CD are largely similar to Cy5 and Cy5.5 homodimers. That is, in each case the absorption spectra are characterized by an intense blueshifted absorption band (compared to the monomer solutions) and CD spectra are characterized by a positive and negative signal at short and long wavelength, respectively. Thus, exciton delocalization is observed in all samples and the interactions between dyes are considerable. Additionally, in all cases the changes in the optical properties compared with the monomers are consistent with H-aggregation, which indicates that both homodimers and even the heterodimer are packing in a similar manner. These results suggest that the packing of the aggregates is maintained independent of the Cy5 or Cy5.5 dye type, which may be related to the similar nature of their chemical structures (**Scheme S1**).

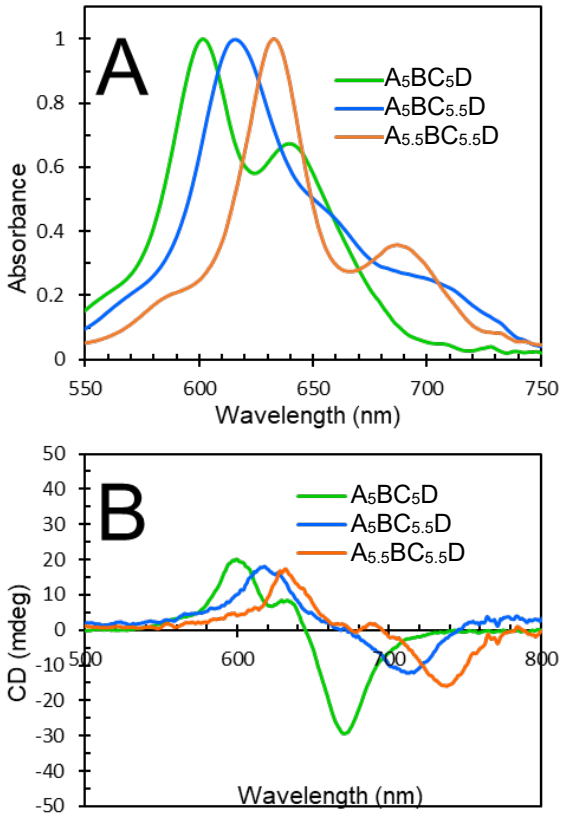


**Figure S8.** Panel **A** and **B** display the absorption (top) and circular dichroism (bottom) spectra of the transverse heterodimer along with Cy5 and Cy5.5 transverse homodimer solutions. The data show that the signature bands of the transverse heterodimer in absorption and CD are similar to and intermediate between Cy5 and Cy5.5 homodimers.

## Section S9. Numerical modeling of transverse hetero- and homo-dimer absorption and circular dichroism spectra

In order to investigate and compare the packing and coupling, we modeled the optical properties (absorption and circular dichroism spectra) of the Cy5 and Cy5.5 transverse hetero- and homo-dimers (**Figure S9.1**). The modeling is performed using the KRM Model Simulation Tool, an in-house software simulation program based on the Kühn-Renger-May (KRM) approach using the Frenkel-Holstein Hamiltonian.[6,8,15]

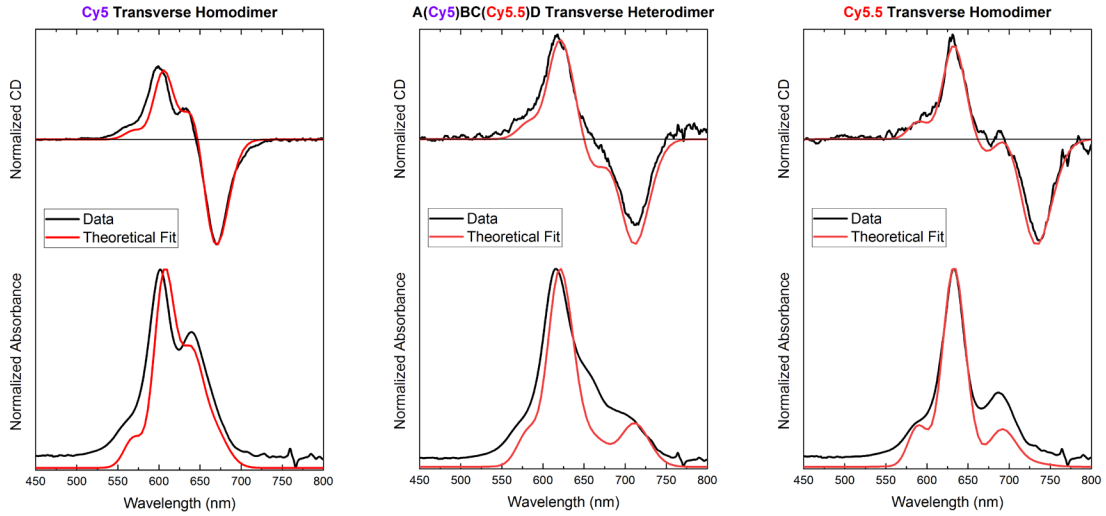


**Figure S9.1.** The absorbance and CD data of Cy5 transverse homodimer (left), transverse heterodimer (middle) and Cy5.5 transverse homodimer (right) along with the theoretical fit are presented here.

The input parameters obtained from the experimental absorption spectrum of the monomers are used in the calculations are listed in **Table S9.1**. The output parameters of monomers and dimers from the modeling are shown in **Tables S9.2** and **S9.6**, respectively. The positions of the TDMs and the orientations of the dye TDMs, via zenith ($\theta_i$) and azimuthal ($\varphi_i$) angles, are given in Tables **S9.3**, **S9.4**, and **S9.5**.

**Table S9.1.** Input fitting parameters for the KRM calculations of Cy5 and Cy5.5 monomers, and dimers.

| | **Monomer** | | | |
|---|---|---|---|---|
| | $A_5BCD$ | $A_{5.5}BCD$ | $ABC_5D$ | $ABC_{5.5}D$ |
| Energy of vibron ($E_v$), meV | 127 | 134 | 136 | 142 |
| Displacement of excited state vibronic potential ($d$), dimensionless units | 0.81 | 0.918 | 0.808 | 0.944 |
| Energy loss damping constant ($\Gamma$), meV | 43 | 43.3 | 39 | 41 |
| Length of transition dipole moment, nm | 1.4 | 1.5 | 1.4 | 1.5 |
| Huang-Rhys factor (dimensionless) | 0.328 | 0.421 | 0.326 | 0.446 |
| | **Dimer** | | | |
| | $A_5BC_5D$ | $A_5BC_{5.5}D$ | $A_{5.5}BC_{5.5}D$ | |
| Energy offset from monomer ($E_{of}$), meV | 12 | 1 | 6.0 | |
| Energy loss damping constant ($\Gamma$), eV | 41.0 | 42.0 | 42.2 | |
| Closest distance between the long axes of any pair of dyes, nm | 0.34 | 0.34 | 0.34 | |

**Table S9.2.** Output parameters of monomers spectra extracted from modeling.

| | **Monomer** | | | |
|---|---|---|---|---|
| | $A_5BCD$ | $A_{5.5}BCD$ | $ABC_5D$ | $ABC_{5.5}D$ |
| Electronic Excitation Energies (E0), eV | 1.90 | 1.78 | 1.90 | 1.78 |
| Transition dipole moment, μ | 13.75 | 14.20 | 13.72 | 16.56 |

**Table S9.3.** KRM fitting outputs describing the orientation of the dye TDMs in dimer $A_5BC_5D$.

| **Dye** | $\theta_i$ **(°)** | $\varphi_i$ **(°)** | $x_i$ **(nm)** | $y_i$ **(nm)** | $z_i$ **(nm)** |
|---|---|---|---|---|---|
| 1 | 63.0 | 0.0 | 0.000 | 0.000 | -0.408 |
| 2 | 100.2 | -8.8 | 0.000 | 0.000 | 0.408 |

**Table S9.4.** KRM fitting outputs describing the orientation of the dye TDMs in dimer $A_5BC_{5.5}D$.

| **Dye** | $\theta_i$ **(°)** | $\varphi_i$ **(°)** | $x_i$ **(nm)** | $y_i$ **(nm)** | $z_i$ **(nm)** |
|---|---|---|---|---|---|
| 1 | 103.1 | 0.0 | 0.000 | 0.000 | -0.316 |
| 2 | 81.7 | -4.1 | 0.000 | 0.000 | 0.316 |

**Table S9.5.** KRM fitting outputs describing the orientation of the dye TDMs in dimer $A_{5.5}BC_{5.5}D$.

| Dye | $\theta_i$ (°) | $\varphi_i$ (°) | $x_i$ (nm) | $y_i$ (nm) | $z_i$ (nm) |
|---|---|---|---|---|---|
| 1 | 91.5 | 0.0 | 0.000 | 0.000 | -0.242 |
| 2 | 101.6 | -3.8 | 0.000 | 0.000 | 0.242 |

**Table S9.6.** Output parameters extracted from KRM calculations of all dimers.

| | Dimer | | |
|---|---|---|---|
| | $A_5BC_5D$ | $A_5BC_{5.5}D$ | $A_{5.5}BC_{5.5}D$ |
| Excitonic hopping parameter ($J_{1,2}$), meV | 69.0 | 95.0 | 115.6 |
| Center-to-center distance ($R$), nm | 0.816 | 0.632 | 0.485 |
| Oblique angle, ($\alpha_{m,n}$) degrees | 38.1 | 21.7 | 10.8 |
| Slip angle 1, ($\theta_s^{m,R}$), degrees | 63.0 | 76.9 | 88.5 |
| Slip angle 2, ($\theta_s^{n,R}$), degrees | 79.8 | 81.7 | 78.4 |

The orientation of transition dipole moment (TDM) vectors of transverse dimers derived from KRM modeling, are presented in **Figure S9.2**. Double-headed arrows represent TDM vectors along the long axis of Cy5 and Cy5.5 dyes. The positions are reported relative to the center of each TDM pair.

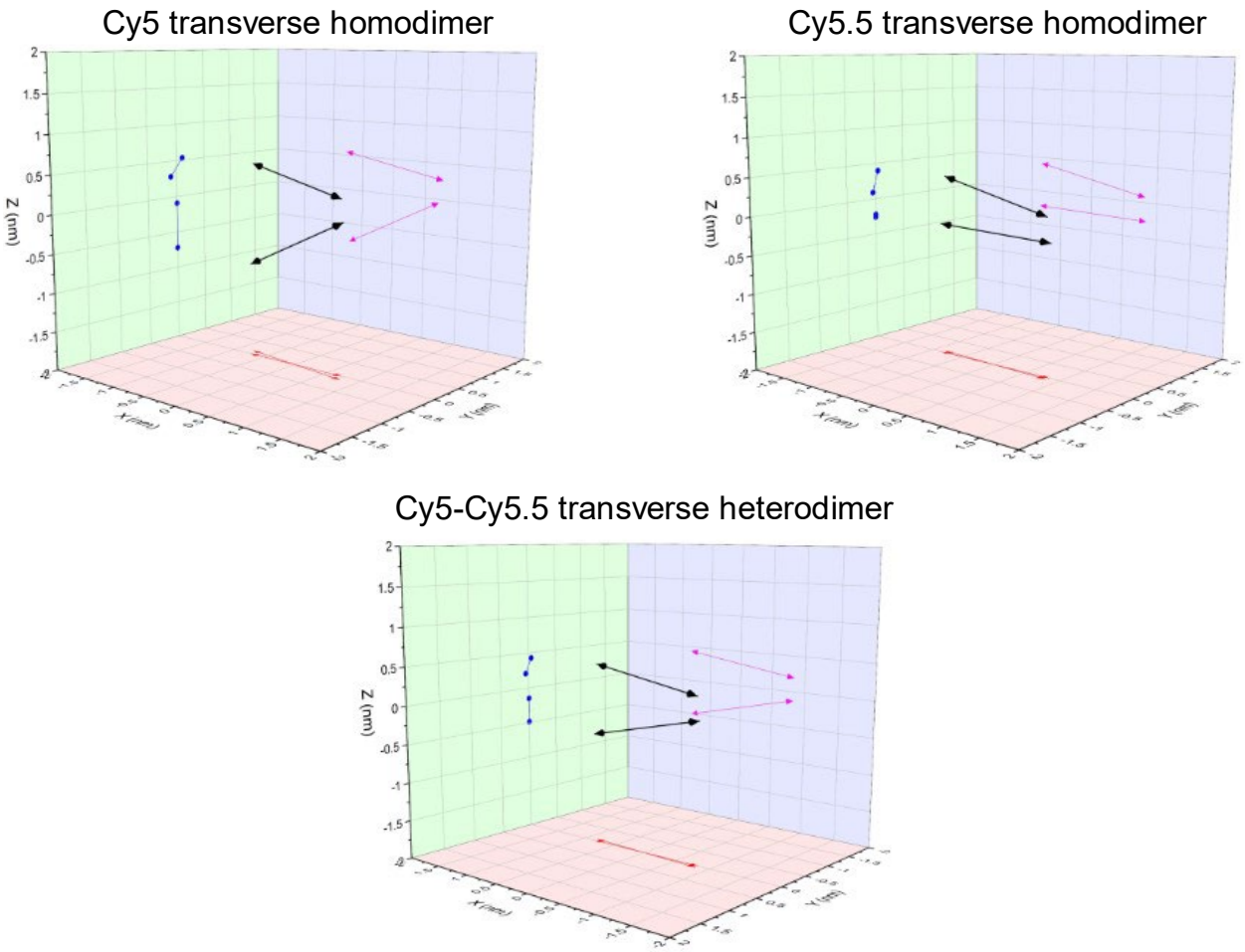


**Figure S9.2.** 3D plot of transition dipole moments (TDMs) of Cy5 transverse homodimer, transverse heterodimers and Cy5.5 transverse homodimers derived from the KRM modeling are presented from the left to right.

**Section S10. Linear combination analysis to model absorption spectrum of adjacent heterodimer solution using monomer solution absorption spectra**

To investigate if there are excitonic interactions between dyes in the adjacent heterodimer solution, we performed a linear combination analysis of its absorption spectrum. In this analysis, we model the absorption spectrum of the adjacent heterodimer by taking a 50/50 linear combination of Cy5 and Cy5.5. The resulting spectrum is presented in **Figure S10**. The sum of monomers spectra (black traces) is overlaid with the Cy5 and Cy5.5 spectra in panel A, and with adjacent heterodimer in panel B. **Figure S10B** shows that a linear combination of monomers is unable to model the data (green trace) and a clear structure is observed in the residual (pink trace). The results of the linear combination analysis can be explained by one of the two following possibilities: (i) in the case of a homogeneous solution, there are excitonic interactions between dyes, or (ii) the solution is heterogeneous (i.e., multiple dye-dye structural configurations are present) and one of these structures is composed of dyes exhibiting excitonic interactions.

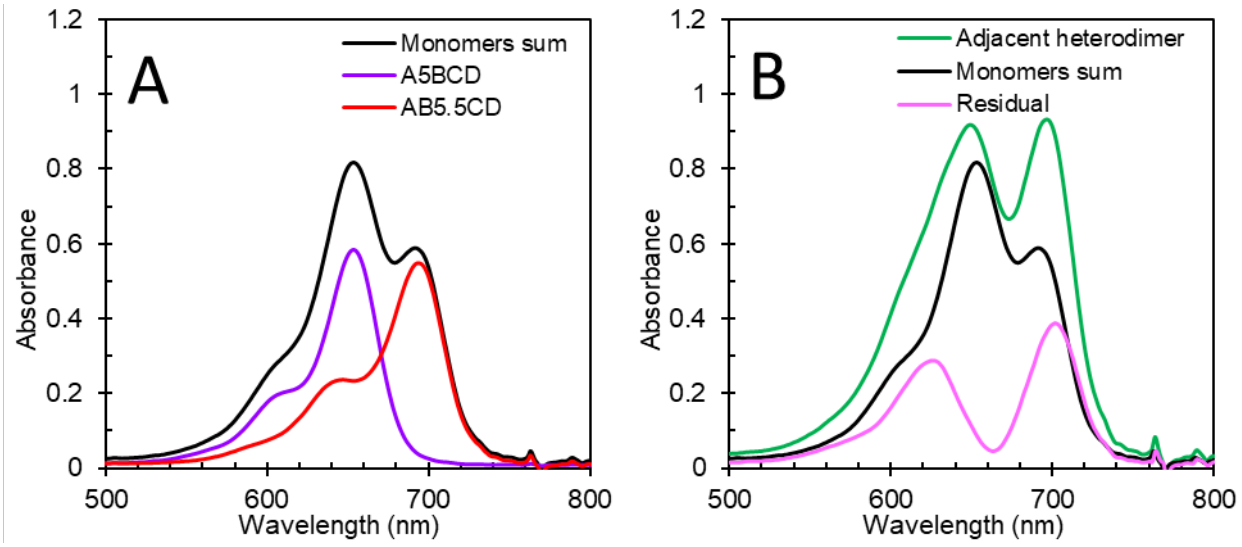


**Figure S10.** Panel **A** shows the absorption spectra of Cy5, Cy5.5 and the sum of 1:1 Cy5 and Cy5.5 monomer solutions (black trace). Panel **B** presents the linear combination analysis to model the absorption spectrum of adjacent heterodimer (green trace) by taking a 50/50 combination of Cy5 and Cy5.5 monomers (black trace). The residual from this modeling is plotted in pink.

**Section S11. Steady-state absorption and fluorescence emission of Cy5 and Cy5.5 monomer solutions**

The absorption and emission spectra of both monomers are presented in **Figure S11.** All spectra are normalized to their corresponding absorption/emission maximum. Two observations can be made from this plot: (i) the fluorescence emission of each dye largely resembles a mirror image of its corresponding absorption spectrum, and (ii) there is a significant spectral overlap between Cy5 emission and Cy5.5 absorption which make these two dyes a suitable candidate as a donor-acceptor pair.

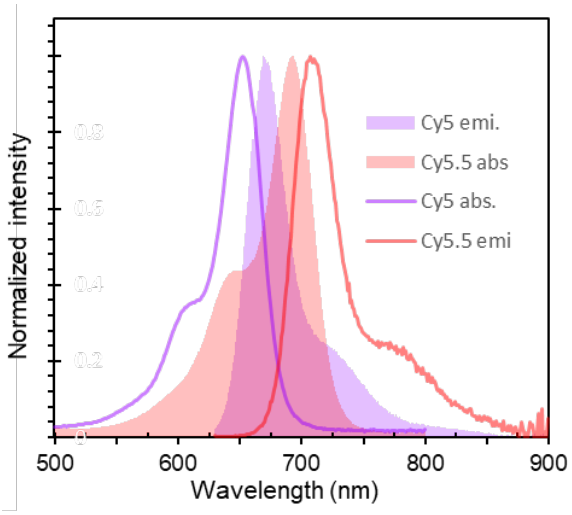


**Figure S11.** Steady state absorption and fluorescence emission of Cy5 and Cy5.5 monomer solutions. Excitation wavelength of 615 nm was used for the fluorescence emission measurements.

In order to quantify the spectral overlap observed in **Figure S11**, we calculated the overlap integral between dyes using the following equation:[12,16]

$$I = \int_0^\infty a_A(\lambda)\, f_D(\lambda)\lambda^4 d\lambda$$

where I is the overlap integral, $a_A(\lambda)$ is the extinction spectrum of acceptor, $f_D(\lambda)$ is the area normalized emission spectrum of the donor and $\lambda$ is the wavelength. The value of I for Cy5 and Cy5.5 was determined to be 2.18 x $10^{-12}$ $M^{-1}$ $cm^3$ (or 2.18 x $10^{16}$ $M^{-1}$ $cm^{-1}$ $nm^4$). In comparison to the spectral overlap of phycoerythrin 545 and chlorophyll a (1.1 x $10^{15}$ $M^{-1}$ $cm^{-1}$ $nm^4$),[16] a natural donor acceptor pair for photosynthesis, Cy5-Cy5.5 exhibits a 20 × enhancement.

**Section S12. Linear combination analysis to model fluorescence emission spectra of transverse and adjacent heterodimer solutions using the emission of monomer solutions**

To gain additional insight into the fluorescence emission spectra of the transverse and adjacent heterodimer solutions, we performed a linear combination analysis of these spectra, results are plotted in **Figure S12**.

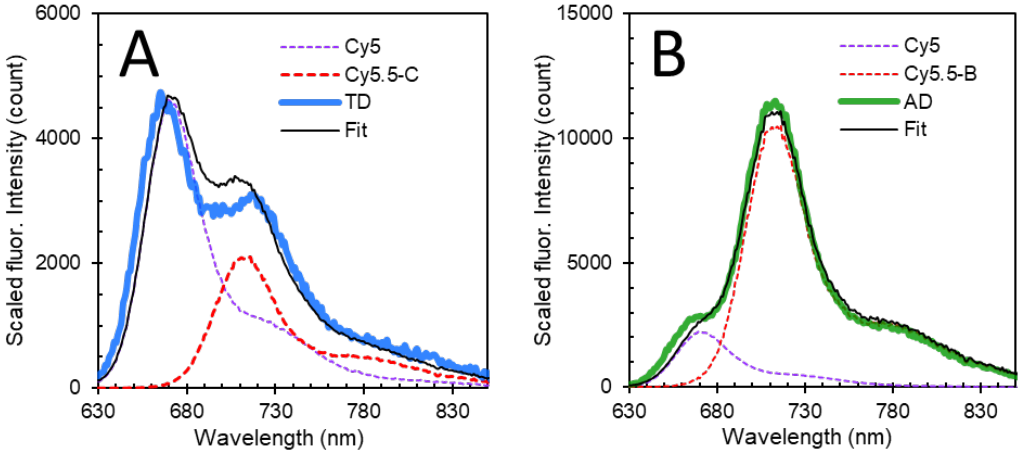


**Figure S12.1.** Linear combination analysis of fluorescence emission of transverse and adjacent heterodimers is presented in panels **A** and **B**, respectively. Both emission spectra were obtained using the same excitation wavelength of 615 nm. It shows that the fluorescence emission of transverse and adjacent heterodimers can fairly be modeled from monomers emission spectra collected at the same excitation wavelength. Thus, the emission from transverse and adjacent heterodimer solutions largely originates from monomers.

In this analysis, we take a linear combination of the Cy5 and Cy5.5 monomer emission spectra to model the emission spectra of transverse and adjacent heterodimer solutions using least-square approach. The first observation is that the heterodimer solution emission spectrum is well modeled by the linear combination of monomer emission spectra, which indicates that the emission from the heterodimer solutions is originating from Cy5 and Cy5.5 monomers.

To gain further insight into the nature of the emission, we further analyzed the relative weighting factor of the Cy5 and Cy5.5 monomer emission needed to model the heterodimer solution emission spectra. Our analysis shows weighting factors of 0.97 and 0.39 for the Cy5 and Cy5.5 monomers emission are needed to model the transverse heterodimer, thus ~3:1 Cy5:Cy5.5 ratio. Similarly, weighting factors of 0.22 and 0.93 for Cy5 and Cy5.5 (i.e., ~1:4 Cy5:Cy5.5) are needed to model the adjacent heterodimer solution. Two key observations can be made from this analysis. First, in the case of the transverse heterodimer the 3:1 Cy5:Cy5.5 monomer emission ratio is similar to the expected Cy5:Cy5.5 monomer emission ratio for a 1:1 mixture of monomers. Specifically, **Figure 2** in the main text displays the Cy5 and Cy5.5 monomer emission spectra scaled according to the solution absorptance (i.e., 1 – transmittance) at the excitation wavelength. Such a scaling procedure accounts for the different fraction of light being absorbed by the different solutions, producing the intensity of light emitted in the case where 100% of the chromophores had absorbed the excitation light. Comparing **Figure S12.1a** with **Figure 2** in the main text, we

can see that the same 3:1 Cy5:Cy5.5 monomer emission ratio needed to model the transverse heterodimer solution emission is very similar to the ratio of monomer emission for the case of a 1:1 mixture of monomers (**Figure S12.2**).

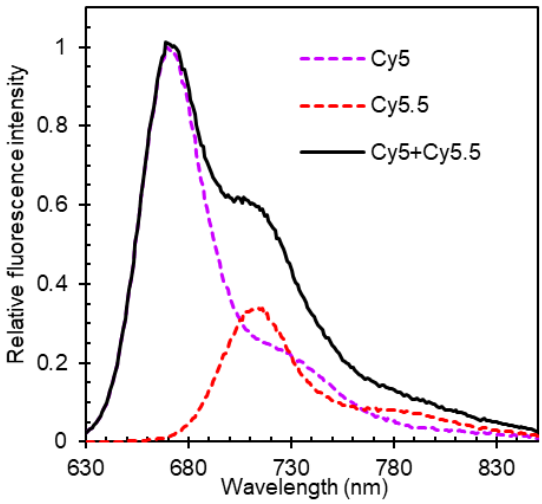


**Figure S12.2.** Cy5 and Cy5.5 monomer emission spectra overlaid with the sum of the two spectra. The excitation wavelength for the measurements of the Cy5 and Cy5.5 monomer emission spectra was 615 nm. The fluorescence emission intensity of each sample was scaled by dividing the intensity by the absorptance (i.e., 1 – transmittance) at the excitation wavelength.

Second, a disproportionately large weighting factor of Cy5.5 (~4×) compared to the Cy5 monomer was needed to model the adjacent heterodimer solution compared to the ratio of the monomer emission intensities when the solution absorptance is accounted for. The former observation is consistent with a small subpopulation of a 50/50 mixture of optical monomers in the transverse heterodimer solution, while the latter observation suggests an energy transfer from Cy5 to Cy5.5 in the adjacent heterodimer solution.

## Section S13. Global target analysis of transient visible absorption of Cy5 monomer, Cy5.5 monomer, and transverse heterodimer solutions

*Global target analysis of transient visible absorption of Cy5 and Cy5.5 monomer solutions*

The transient visible absorption of the Cy5 and Cy5.5 monomer solutions, presented in the main text (**Figure 3A** and **3B**), were analyzed via a global and target analysis using 2-component kinetic schemes for both monomers (**Figure S13.1**).

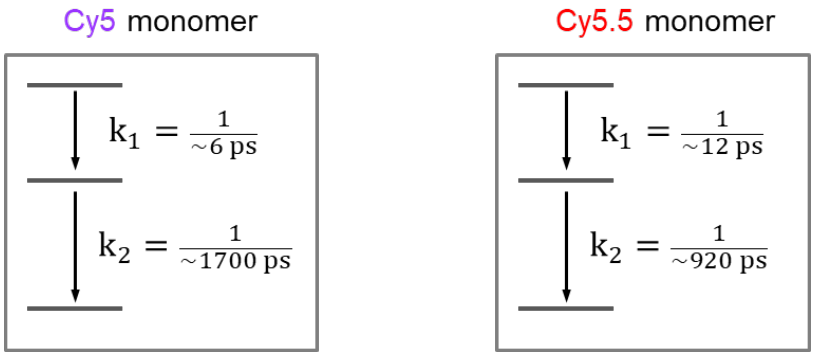


**Figure S13.1.** Kinetic schemes used to model the Cy5 and Cy5.5 monomers.

We modeled these data using both 1- and 2-components. We considered the simplest model that best describes the data. Therefore, we started with a single component. It shows that using a single component can fairly model the data in the longer time delay regions, but early time delay regions (~0-10 ps time delay region) are poorly modeled for both monomers. For example, the kinetic traces at 660 and 700 nm of Cy5 and Cy5.5, respectively, show discrepancies between the data and fit in the early time delay regions. Therefore, we introduced another kinetic component to model the data for both monomers. The results are displayed in **Figures S13.2-S13.4**.

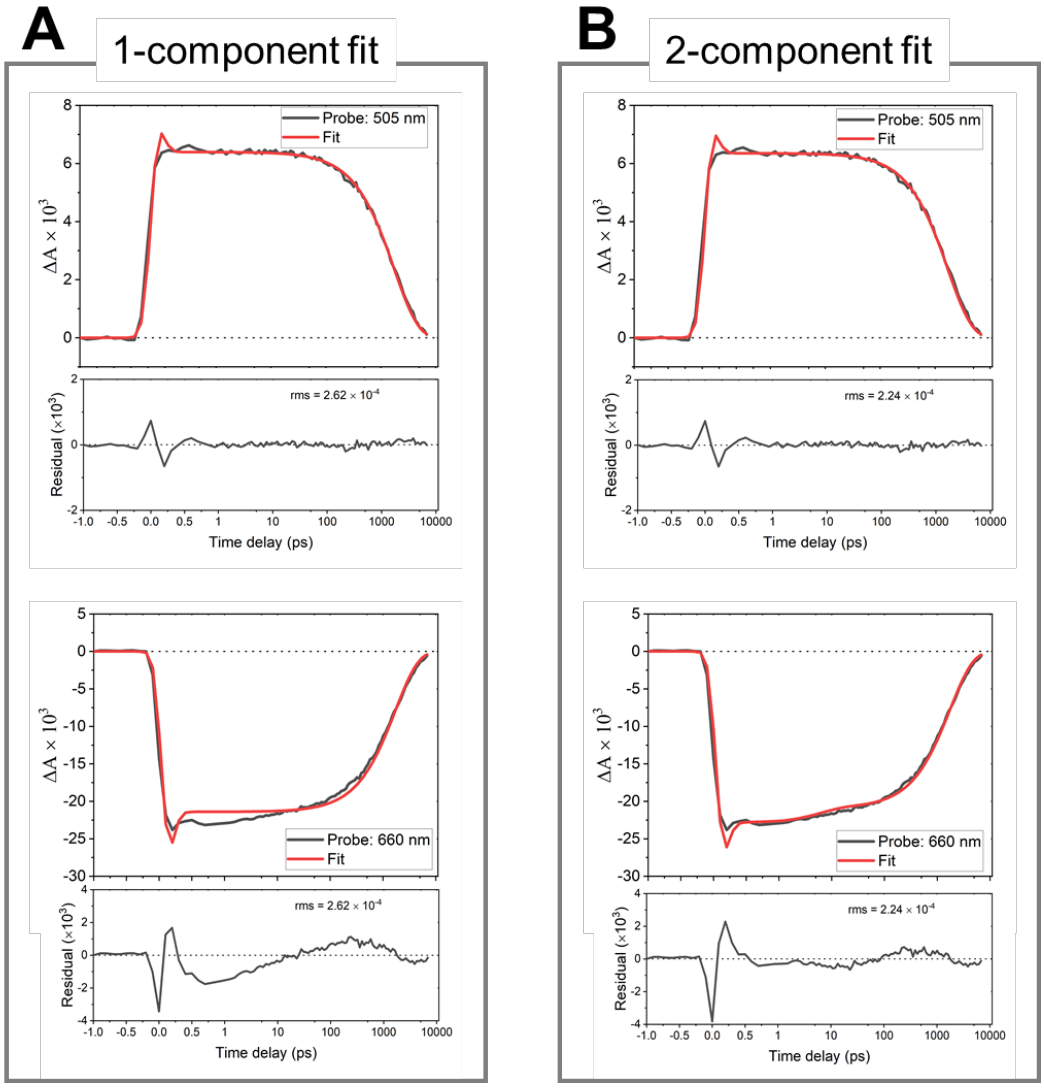


**Figure S13.2.** Selected transient kinetics traces of excited state absorption and ground state bleach of Cy5 monomer at 505 and 660 nm, respectively, along with fits, rms values, and residuals from the global and target analysis. Panel **A** and **B** show the fits, rms values, and residuals associated with 1- and 2-component kinetic schemes, respectively, for both kinetics traces.

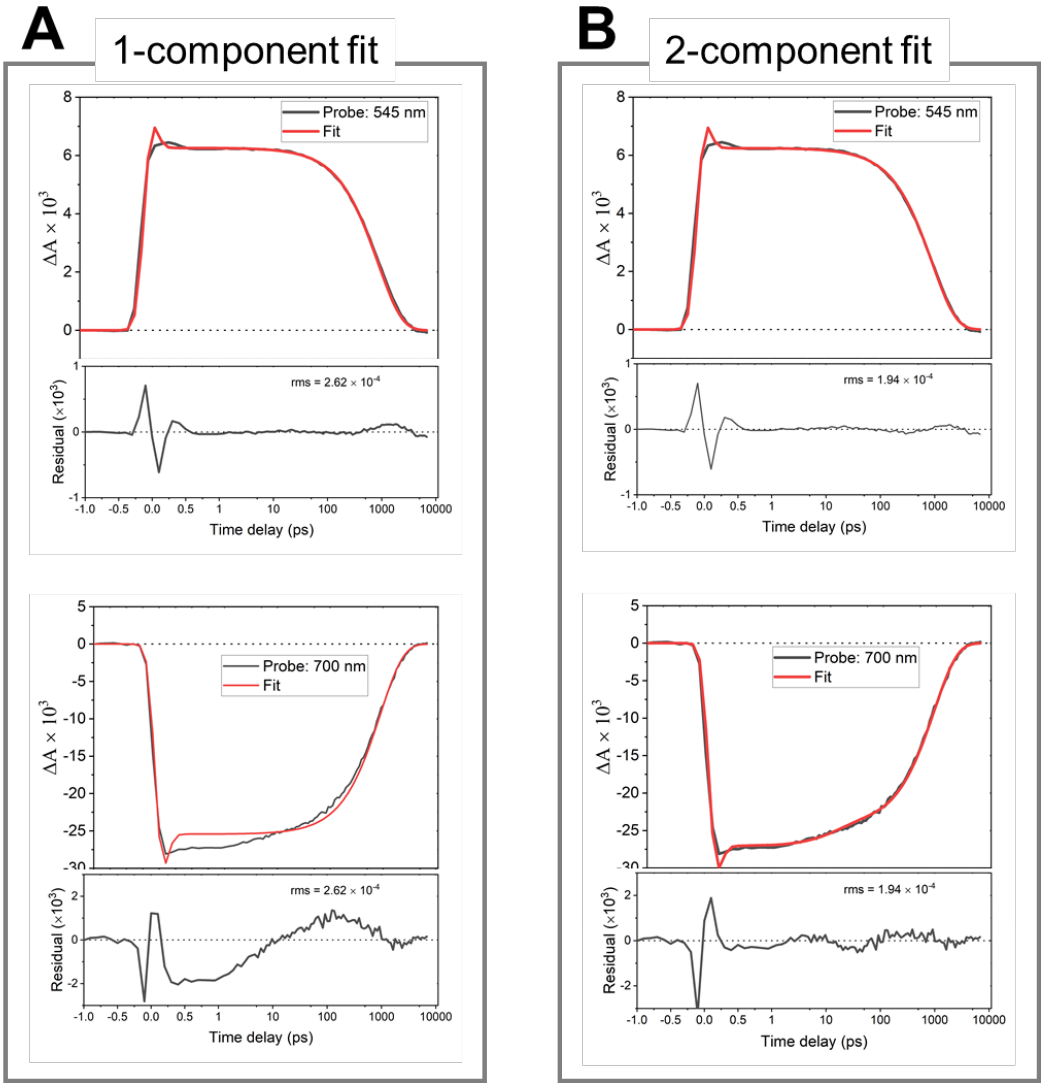


**Figure S13.3.** Selected transient kinetics traces of excited state absorption and ground state bleach of Cy5.5 monomer at 545 and 700 nm, respectively, along with fits, rms values, and residuals from the global and target analysis. Panel **A** and **B** show the fits, rms values, and residuals associated with 1- and 2-component kinetic schemes, respectively, for both kinetics.

Clearly, the 2-component model better describes the data (i.e., **Figures S13.2** and **S13.3**). Based on the redshift of the stimulated emission features observed in progressing from SAS1 to SAS2 in both the Cy5 and Cy5.5 monomer solutions (**Figure S13.4**), we assign the first component (i.e., $k_1$) to an energy relaxation step of the lowest-energy excited state, i.e., colloquially known as a dynamic Stokes shift. We assign the second component (i.e., $k_2$) to the excited-state lifetime of Cy5 and Cy5.5 monomers. The timescale of the first process of each of them is ~10 ps, while the lifetimes of Cy5 and Cy5.5 are ~1700 and ~920 ps, respectively.

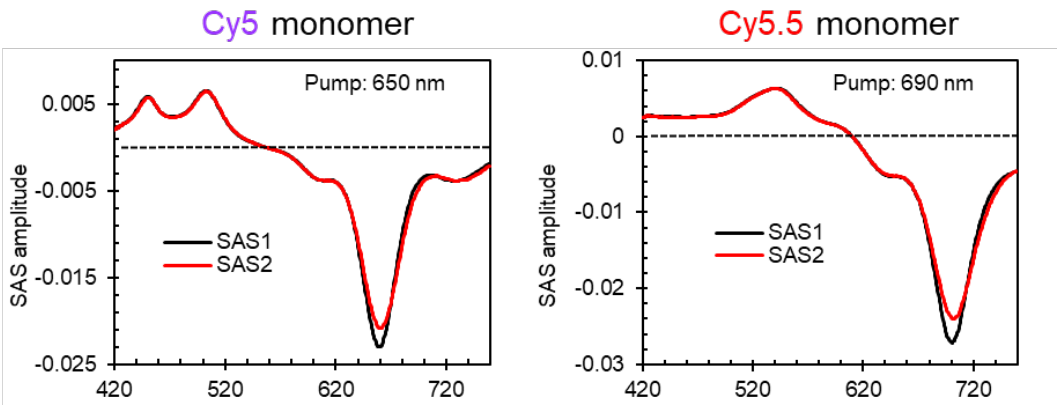


**Figure S13.4.** Species-associated spectra of Cy5 and Cy5.5 monomers derived from global and target analysis using a 2-component kinetic scheme. Species-associated spectra SAS1 (black) and SAS2 (red) attributed to dynamic Stokes shift and excited-state lifetime, respectively, for both monomers.

*Global target analysis of transient visible absorption of transverse dimer solution*

The transient visible absorption of the transverse heterodimer solution, presented in the main text (**Figure 3C**), was analyzed via a global and target analysis using a 3-component kinetic scheme (**Figure S13.5**).

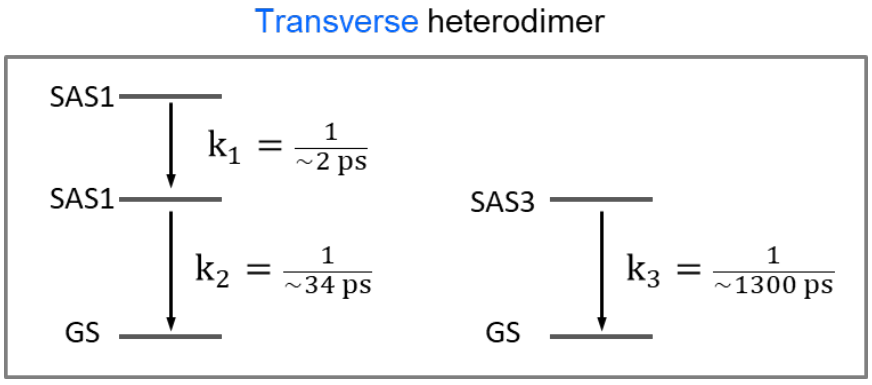


**Figure S13.5.** Kinetic scheme used to model the transverse heterodimer solution.

We modeled the transverse heterodimer data using both 2- and 3-component schemes. Again, we considered the simplest model that best describes the data. However, from the pump wavelength dependent measurements of the transverse heterodimer solution, we determined that the solution was heterogeneous, i.e., composed of a mixture of strongly coupled structures and

optical monomers (see e.g. **Sections S15**). Thus, we started with a 2-component model instead of 1-component. It shows that 2 parameters, which account for a few picosecond timescale and tens of picosecond timescale dynamics, cannot fairly model the data in longer time delay regions. For example, kinetic traces at 615 and 710 nm, respectively, show discrepancies between data and fit. Therefore, because the long time delay regions in the vicinity of where we expect the optical monomers to contribute was not modeled well (i.e., nanosecond timescale), we introduced an additional, third component to account for the optical monomers. In this case, we treat the monomers together and, since they should be present in the solution in a 1:1 ratio, we treat their lifetime as the average lifetime of the two monomers, i.e., ~1.3 ns to model the data, results are displayed in **Figures S13.6** and **S13.7**.

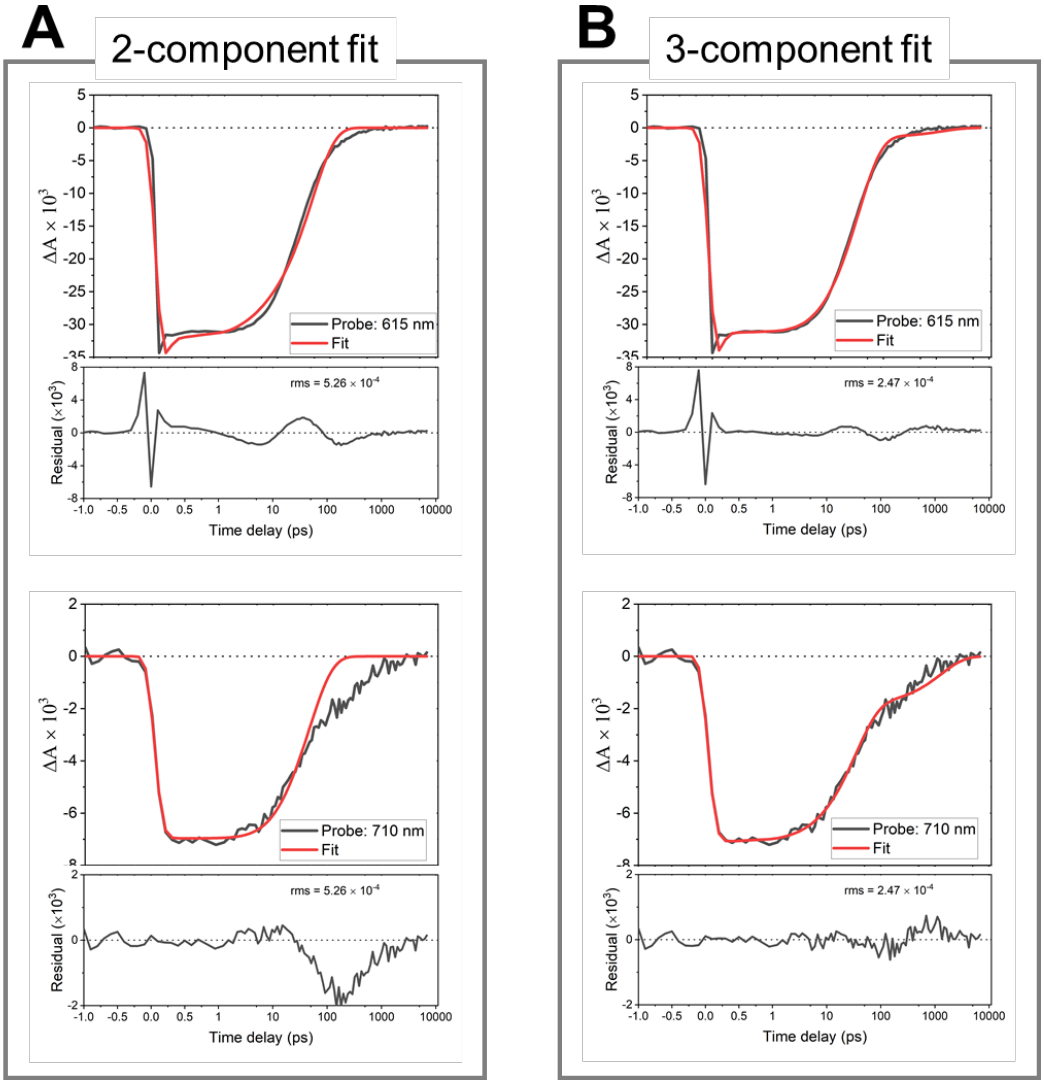


**Figure S13.6.** Selected transient kinetics traces of ground state bleach of transverse heterodimer at 615 and 710 nm, respectively, along with fits, rms values, and residuals from the global and target analysis. The fits, rms values, and residuals associated with 2- and 3-component kinetic schemes are presented in left and right columns, respectively.

It is evident that the 3-component model better describes the data (e.g., **Figure S13.6**). Based on the trend in the SAS1 and SAS2 (**Figure S13.7**), which compare well with literature precedents,[7] we assign SAS1 to the relaxation of the lowest-energy excited state. Specifically, we observe changes to the ESA bands below ~540 nm, which we attribute to changes of the excited-state electronic structure of the transverse heterodimer. Notably, these observations are inconsistent with the interpretation of energy transfer between Cy5 and Cy5.5. For example, SAS1 exhibits a single ESA band at ~520 nm, which does not match the ~540 nm ESA band of Cy5.5, and SAS2 exhibits a single band at ~470 nm, which does not match either of the two Cy5 ESA bands at ~450 and ~500 nm. Furthermore, the signal at ~520 nm, which, although not matching, is in the vicinity of the Cy5.5 ESA band, decays and the feature at ~470 nm, which, although not matching, is in the vicinity of the Cy5 ESA bands, grows in, which is inconsistent with energy transfer between Cy5 and Cy5.5. Rather, these spectral changes are consistent with those expected of strongly excitonically interacting dyes (see e.g. **Figure 1** and **Section S6**) and bear a striking resemblance to previous measurements on Cy5 homoaggregates.[7] The global target analysis derives a time constant of ~2 ps for these dynamics. We assign the second component (i.e., SAS2) to the lowest-energy excited state of the transverse heterodimer structure before it relaxes to the ground state, with a ~34 ps time constant derived for the excited-state lifetime of the transverse heterodimer.

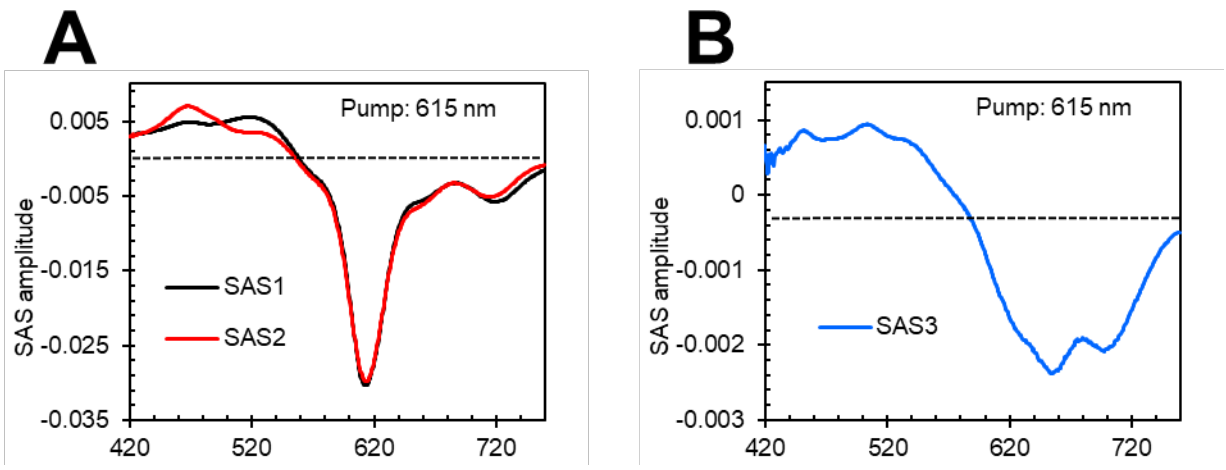


**Figure S13.7.** Species-associated spectra of transverse heterodimer solution derived from global and target analysis using a 3-component kinetic scheme. Panel **A** shows the species-associated spectra SAS1 (black) and SAS2 (red) those are attributed to dynamic Stokes shift and excited-state lifetime of strongly coupled structure, respectively. Panel **B** shows SAS3 (blue trace) which is attributed to the optical monomers present in the solution.

As **Figure 13.7** shows, the third component (i.e., SAS3) with a time constant of ~1.3 ns looks very similar to a linear combination of the transient absorption spectra of Cy5 and Cy5.5 monomers (**Figures 3A** and **3B** in the main text), which is consistent with the interpretation of the presence of a small subpopulation of optical monomers in the transverse heterodimer solution. Specifically, prominent ESA bands at ~455 and 505 nm and GSB/SE band at ~660 nm attributable

to Cy5 are observed in SAS3, along with prominent ESA band at ~540 nm and GSB/SE at ~700 nm attributable to Cy5.5.

**Section S14. Analysis of Cy5 and Cy5.5 monomer radiative and nonradiative decay rates**

In this section, we determine the radiative and nonradiative decay rate of Cy5 and Cy5.5 monomers from the observed decay rates and fluorescence quantum yield values. The observed decay rate is obtained from the transient absorption measurement by analyzing the data via global target analysis (**Section S13**). Additionally, the fluorescence quantum yield (**Table 1** in the main text) is measured via steady-state fluorescence emission spectroscopy.

Fluorescence quantum yield is related to the radiative decay rate by the following equation:

$$\Phi_F = \frac{k_r}{k_{obs}}$$

Here, $\Phi_F$ is fluorescence quantum yield, $k_{obs}$ and $k_r$ are observed and radiative decay rates, respectively. At the same time, $k_{obs}$ is the sum of $k_r$ and nonradiative decay rate ($k_{nr}$), and is given by the following equation:

$$k_{obs} = k_r + k_{nr}$$

Using these equations, we calculated the radiative and nonradiative decays rates of Cy5 and Cy5.5 monomers, and the results are presented in **Table S14**.

**Table S14.** Calculated radiative and nonradiative decay rate of Cy5 monomer and Cy5.5 monomer

| **Cy5 monomer** | | | **Cy5.5 monomer** | |
|---|---|---|---|---|
| $\boldsymbol{\Phi_F}$ | 0.45 | | 0.28 | |
| $\boldsymbol{\tau_{obs}}$ | 1700 | ps | 920 | ps |
| | | | | |
| $\boldsymbol{k_r}$ | 2.65 x $10^8$ | $s^{-1}$ | 3.04 x $10^8$ | $s^{-1}$ |
| $\boldsymbol{k_{nr}}$ | 3.24 x $10^8$ | $s^{-1}$ | 7.83 x $10^8$ | $s^{-1}$ |

**Table S14** shows that while the radiative decay rate of the monomers is about the same, the nonradiative decay rate of the Cy5.5 monomer is more than two times that of the Cy5 monomer.

## Section S15. Internal conversion is primary nonradiative decay pathway of the transverse heterodimer

**Figure 3** in the main text shows that the transverse heterodimer decays with a lifetime of ~31 ps, which is very rapid compared with the ~1.7 ns and ~930 ps lifetimes of the Cy5 and Cy5.5 monomers, respectively. These results are consistent with the low fluorescence quantum yield (FQY) of the transverse heterodimer solution, measured to be 0.01, which is small compared to the FQY values of 0.45 and 0.28 for Cy5 and Cy5.5 monomer solutions, respectively. Thus, the transverse heterodimer decays to the ground state nonradiatively. In this section, we discuss the primary nonradiative decay pathway of the transverse heterodimer.

Transient absorption spectroscopy is an excellent probe of nonradiative decay pathways because the method probes both "bright" and "dark" excited states. In past work, we showed that nonradiative decay via internal conversion explained the rapid quenching of photoexcitations in dimer, trimer, and tetramer aggregates consisting of strongly excitonically interacting Cy5 dyes.[7,17] Here, the transverse heterodimer consists of two strongly interacting and chemically distinct dyes, Cy5 and Cy5.5. Thus, we revisit the possibility of distinct pathways, including intersystem crossing, photoisomerization, charge transfer, and internal conversion directly from $S_1$ to $S_0$, as explaining the nonradiative decay of the transverse heterodimer.

Intersystem crossing and photoisomerization are immediately ruled out as the primary ground-state bleach feature at ~615 nm, which maps onto the steady-state absorption spectrum of the transverse heterodimer, decays complete to baseline with a time constant of ~31 ps. In contrast, intersystem crossing and photoisomerization for Cy5 attached to DNA have been reported to take place on the microsecond timescale.[18] Here, we assume that the timescale of intersystem crossing and photoisomerization are not dramatically changed for Cy5.5 with the presence of the two additional aryl groups (**Scheme S1**).

Thus, we are left to consider charge transfer and/or internal conversion directly from $S_1$ to $S_0$. In past work, we argued against the charge transfer pathway, as the aggregates consisted of the same dye.[17] Here, the aggregates consist of two chemically distinct dyes, and so, charge transfer may be feasible. In the present work, we benefit from transient absorption across a wide visible (VIS) and near-infrared (NIR) probing window (**Figure S3.2.3**). In the case of electron transfer between Cy5 and Cy5.5 we might expect, to zero order, the electron to be transferred from Cy5 to Cy5.5. Thus, the Cy5 is oxidized and should exhibit spectral signatures of the radical dication. In a seminal work by Lenhard and Cameron, the spectral characteristics of the oxidized forms of numerous cyanine derivatives, including Cy5, were surveyed. For the radical dication of Cy5, the authors identified distinct absorption bands at ~494 and 944 nm. Thus, if electron transfer is taking place, we can expect to observe these distinct absorption bands in the transient absorption measurement. **Figure S15** displays selected transient VIS and NIR absorption spectra of the transverse heterodimer solution at time delays of 0 fs, 800 fs, and 200 ps. Clearly, there are no absorption features on any of these timescales that can be attributed to the Cy5 radical dication. Thus, we rule out the possibility of charge transfer explaining the nonradiative decay in the transverse heterodimer.

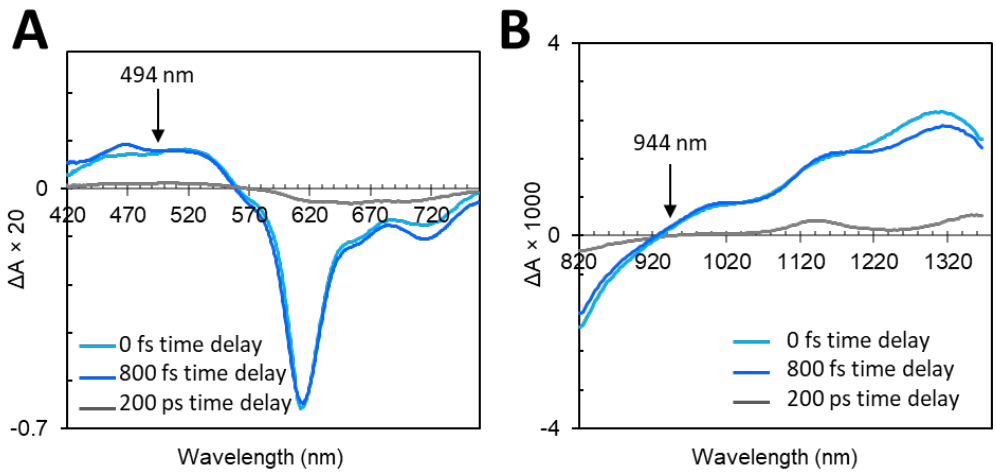


**Figure S15.** Selected transient (**A**) visible and (**B**) near-infrared absorption of the transverse heterodimer solution pumped at 615 nm. Overlaid in panels **A** and **B** are arrows pointing to the expected visible and near-infrared absorption bands, respectively, of the oxidized form of Cy5, i.e., the radical dication.

Thus, we are left with the possibility of internal conversion directly from $S_1$ to $S_0$ to explain the nonradiative decay of the transverse heterodimer. This interpretation is consistent with the near constant GSB over the picosecond timescale, which subsequently decays completely on the tens of picosecond timescale (**Section S13**).

**Section S16. Pump wavelength dependent transient visible absorption of transverse heterodimer solution suggests the solution is heterogeneous**

To shed insight into the origin of the Cy5 and Cy5.5 monomer emission observed in the transverse heterodimer solution, we performed pump wavelength-dependent TA measurements by pumping the heterodimer solution at wavelengths of 615, 650, and 690 nm. The results are shown in **Figure S16A**. The TA spectra of the transverse heterodimer solution exhibits spectral features weighted by different amplitudes when pumping at different wavelengths. For example, when the solution is excited with 615 nm, the feature associated with the strongly coupled structure at ~615 nm is more pronounced, but when the solution is pumped excited at 650 nm, negative features at ~660 and ~700 nm grow in intensity while the negative feature at ~615 nm is reduced. These negative peaks at ~615, ~660 and ~700 nm are assigned to the GSB of the strongly coupled structure, the GSB/SE of Cy5 monomer, and the GSB/SE of Cy5.5 monomer, respectively. Similarly, when excited at 690 nm, the spectral signatures of the strongly coupled structure is further reduced, the GSB/SE features of the Cy5 monomer is no longer present, and the signal at ~700 nm associated with Cy5.5 GSB/SE is the most dominant feature. We also plotted two kinetic traces along with the fits at two probe wavelengths (615 and 660 nm) from the TA surface plot of transverse heterodimer solution, pumped at 615 nm, in **Figure S16B**. Figure shows two different kinetics (~31 ps and ~1.3 ns) at two different probe wavelengths, which provides additional evidence that the solution contains multiple optically-active populations. Overall, these pump wavelength dependent TA measurements suggest that the transverse heterodimer solution is heterogeneous, consisting of a large population of strongly-coupled structures and a smaller subpopulation of monomers, which could be of either static or dynamic origin, as described in detail previously.[7,19]

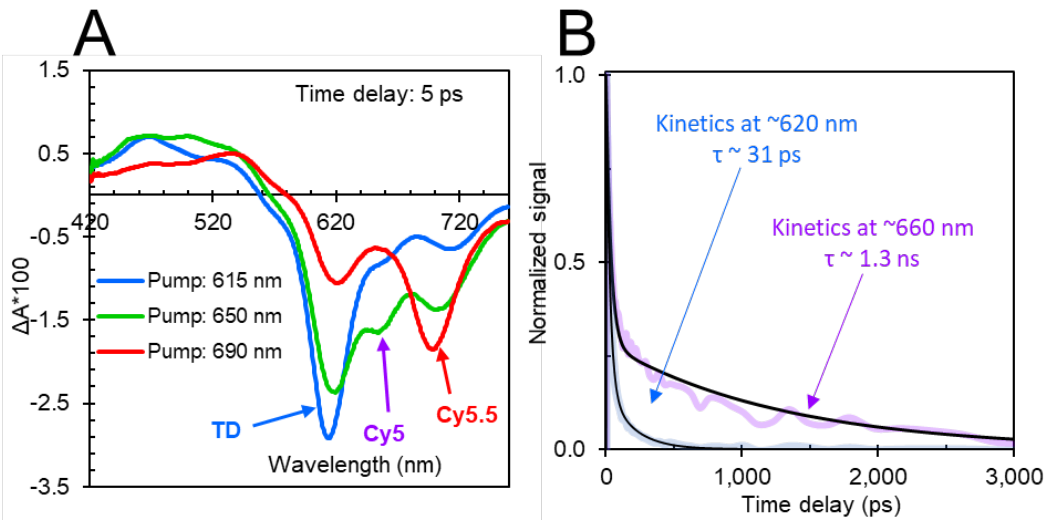


**Figure S16.** Panel **A** is the overlay of transient visible absorption spectra of the transverse heterodimer solution selected at 5 ps with pump wavelengths of 615 (blue), 650 (green), and 690

(red) nm, respectively. The data show that negative-going signals in the vicinity of GSB/SE signatures of Cy5 and Cy5.5 monomers are more pronounced when the transverse heterodimer solution is pumped at 650 and 690 nm, which correspond to the absorption maxima of Cy5 and Cy5.5, respectively. Panel **B** shows the kinetics at ~620 and ~660 nm of transverse heterodimer solution, pumped at 615 nm.

**Section S17. An alternative way of visualizing the Cy5 signals in the transient visible absorption of the adjacent heterodimer solution**

In this section, we present an alternative way of visualizing the Cy5 signals in the transient visible (VIS) absorption of the adjacent heterodimer solution (see e.g. **Figure 4B** in the main text). **Figure S17** displays transient VIS absorption spectra of the adjacent heterodimer solution at selected time delays of 0 and 2 ps overlaid with transient VIS absorption spectra of Cy5 and Cy5.5 monomer solutions obtained at a time delay of 2 ps. Clearly, the transient VIS absorption spectrum of the adjacent heterodimer solution at a time delay of 0 ps exhibits signals in the vicinity of the two Cy5 monomer ESA bands at ~450 and ~500 nm, which decreases in intensity in the corresponding spectrum at a time delay of 2 ps. Furthermore, the transient VIS absorption spectrum of the adjacent heterodimer solution at a time delay of 0 ps exhibits negative-going amplitude in the vicinity of the overlapping ground-state bleach and stimulated emission feature of Cy5 at ~660 nm, which decreases in intensity in the corresponding spectru at a time delay of 2 ps. As explained in detail in the main text, these observations, combined with simultaneous growth of Cy5.5 monomer features, are consistent with energy transfer between Cy5 and Cy5.5 on the few hundred femtosecond timescale.

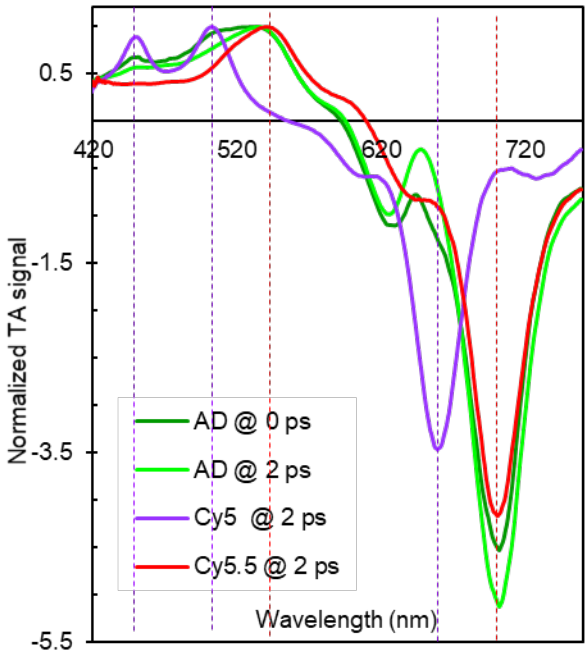


**Figure S17.** Selected transient visible absorption spectra of adjacent heterodimer solution at time delays of 0 and 2 ps along with corresponding spectra of Cy5 and Cy5.5 monomer solutions at a 2 ps time delay. Each spectrum is normalized to the amplitude of its maximum ESA band. Vertical dashed purple and red lines are included to highlight specific excited-state absorption and overlapping ground-state absorption and stimulated emission bands associated with Cy5 and Cy5.5 monomers, respectively.

**Section S18. Transient visible absorption of adjacent heterodimer solution excited at 650 nm over the full time window**

To understand the long-time dynamics of the adjacent heterodimer solution, we performed a TA measurement of the solution at 650 nm pump over an 8 ns time delay window (**Figure S18A**). A selected spectrum at 700 ps is shown in panel **C** along with a TA spectrum of the Cy5.5 monomer solution. Because these spectra look similar, we assign the long-time (700 ps) TA spectrum of the adjacent heterodimer solution to that of Cy5.5 monomers. Additionally, we performed a global target analysis to model the adjacent heterodimer TA spectra using a 3-component model (**Figure S18B**). Analysis indicates that the longest lifetime has a time constant of ~700 ps, which we assign to long-lived Cy5.5 monomers. The kinetics trace at ~700 nm along with the fit are presented in panel **D**. The time constant of ~700 ps is very similar to the 930 ps lifetime of the Cy5.5 monomer (**Figure 3** in the main text).

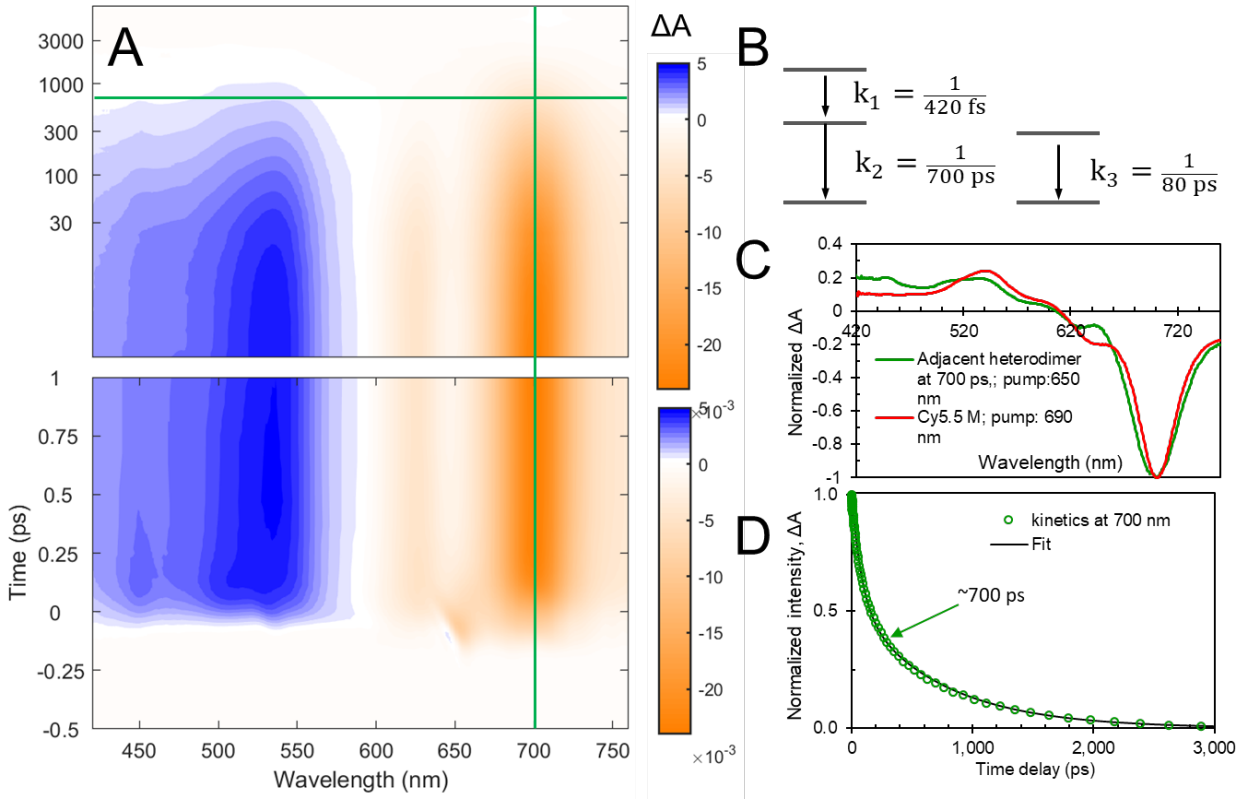


**Figure S18**. Panel **A** displays the transient visible absorption surface plot of the adjacent heterodimer solution pumped at 650 nm. Panel **B** shows the 3-components kinetic scheme used in the global target analysis to model the data. Panel **C** is the overlay of Cy5.5 monomer and the selected spectrum at 700 ps from the adjacent heterodimer solution. Panel **D** shows the longest kinetic trace at 700 nm with a decay constant of (1/700) $ps^{-1}$.

In addition to the monomer component (~700 ps time constant) and an early-time component associated with the energy transfer between Cy5 and Cy5.5 (~420 fs time constant), a

third component with a time constant of ~80 ps was required to model the data. We assign the third component to the sub-population of dimers consisting of excitonically interacting dyes. The short lifetime is consistent with the quenching observed in the case of the transverse heterodimer, which exhibits a lifetime of ~34 ps (**Section S13**).

The extent to which the third component contributes to the overall decay can be evaluated by considering that, at a time delay of ~700 ps, the total signal has decayed to ~20% of its initial value. In the case of the subpopulation of dimers consisting of non-excitonically interacting dyes, we expect essentially unity energy transfer (see e.g. main text) followed by relaxation with a lifetime of the order of that of the Cy5.5, which we measure here to be ~700 ps. In this case, we expect the total signal to decay to 37% of its initial value by 700 ps. Obviously, the sub-population of dimers consisting of excitonically interacting dyes contributes appreciably to the measurement. These results are consistent with the linear combination analysis of the adjacent heterodimer solution absorption spectrum, which indicated a considerable residual amplitude associated with the sub-population of dimers consisting of excitonically interacting dyes (**Section S10**).

Further, the results above help rationalize the value of 0.11 measured for the fluorescence quantum yield (FQY) of the adjacent heterodimer solution, which does not match the value of 0.28 measured for the Cy5.5 monomer solution. Specifically, in the case of unity energy transfer from Cy5 to Cy5.5, followed by excited-state relaxation of Cy5.5, we expect the FQY of the adjacent dimer solution to be equivalent to that of the FQY of the Cy5.5 monomer solution, i.e., 0.28. However, an appreciably smaller value is measured, i.e., 0.11. We rationalize this by considering that, at the excitation wavelength of 615 nm where the measurements were performed, the source excites a considerable amount of both sub-populations of dimers consisting of excitonically interacting dyes that quench and exhibit a low FQY and sub-populations of dimers consisting of non-excitonically interacting dyes that undergo unity energy transfer and exhibit a high FQY. In past work,[17] we provided general expressions that describe the FQY of both homogeneous and heterogeneous solutions. Thus, if nearly equivalent amounts of each sub-population were excited, we might expect an FQY value for the adjacent dimer solution that is nearly one-half of the FQY value of the Cy5.5 monomer solution, which is nearly equivalent to that observed.

**Section S19. Transient near-infrared absorption of Cy5 and Cy5.5 monomer solutions**

To investigate the excited-state near-infrared (NIR) electronic structure of the Cy5 and Cy5.5 monomers, we performed transient NIR absorption measurements on the Cy5 and Cy5.5 monomer solutions. Surface plots and selected spectra are presented in **Figure S19**. Selected spectra in panel **C** show that the Cy5 and Cy5.5 monomers have distinct excited-state absorption (ESA) bands peaking at ~1130 and ~1360 nm, respectively. These distinct ESA bands of Cy5 and Cy5.5 monomers, which we assign to an $S_1 \rightarrow S_m$ transition, confer selectivity between Cy5 and Cy5.5 monomers in the NIR spectral region due to their distinct chemical structure (**Scheme S1**).

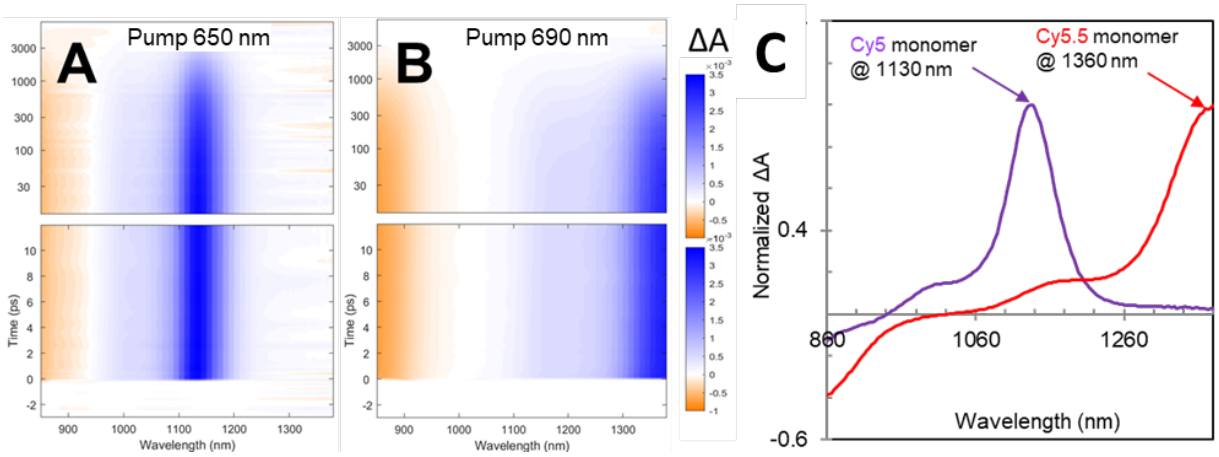


**Figure S19.** Panels **A** and **B** display the transient near-infrared absorption of Cy5 and Cy5.5 monomer solutions. Selected spectra for Cy5 and Cy5 monomer solutions at 2 ps time delay are shown in panel **C**.

**Section S20. Global target analysis of transient near-infrared absorption of adjacent heterodimer solution pumped at 650 nm**

To gain insight into the timescale of the energy transfer between Cy5 and Cy5.5 in the adjacent dimer, a global target analysis was performed on transient near-infrared absorption of adjacent dimer solution excited at 650 nm. The analysis was performed on three independent measurements. **Figure S20.1** displays the two-component kinetic scheme used to model the data.

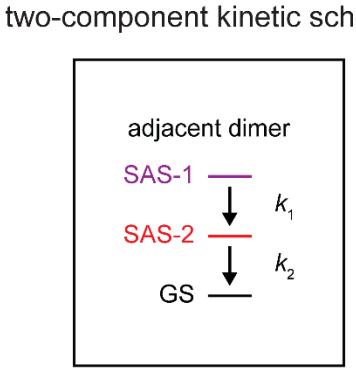


**Figure S20.1.** Two-component kinetic scheme used for global target analysis of the adjacent dimer solution excited at 650 nm. The two-component kinetic scheme accounts for: (i) a short-lived component associated with an appreciable fraction of directly excited Cy5, and (ii) a long-lived component associated entirely with Cy5.5. The short-lived component also exhibits an appreciable amount of Cy5.5 that may arise either from direct excitation of Cy5.5 or the transfer of energy from Cy5 to Cy5.5 during the pump pulse overlap.

**Figure S20.2** displays the data, fits, and residuals for the adjacent dimer solution excited at 650 nm when applying the two-component kinetic scheme. $k_2$ in the kinetic scheme was fixed to the value of (1/80) $ps^{-1}$ (see e.g. **Section S18**), while $k_1$ was allowed to float.

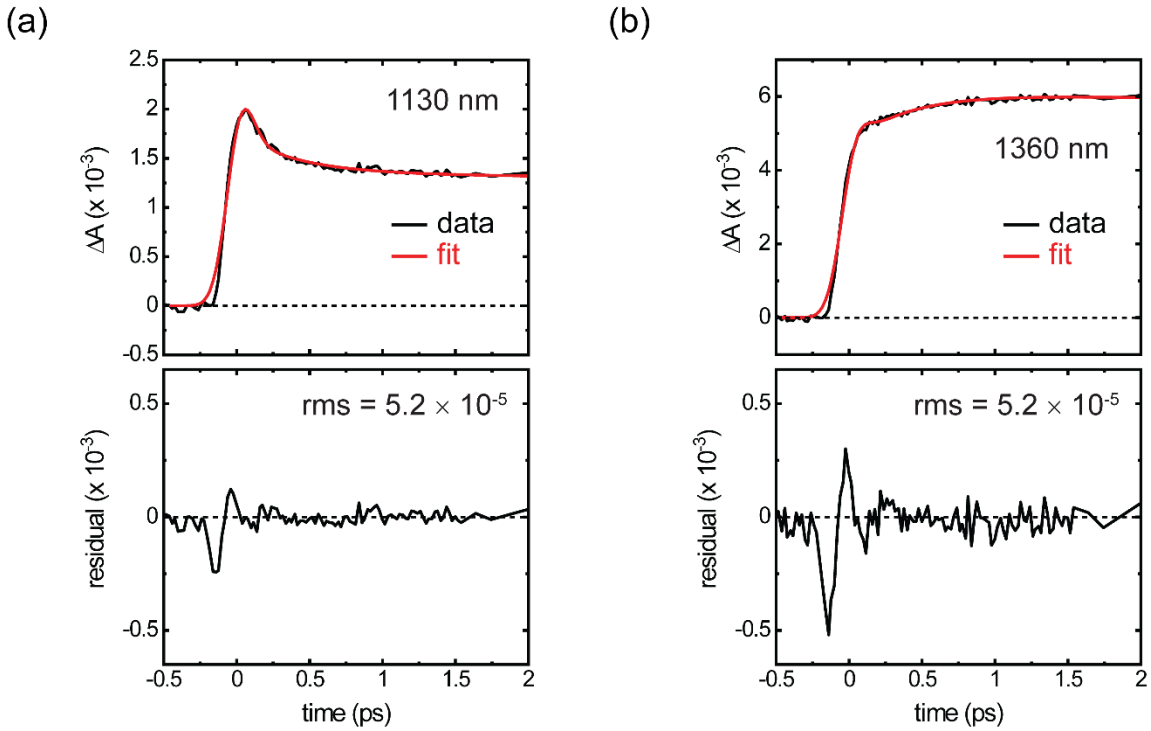


**Figure S20.2.** Selected transient kinetics traces for the adjacent dimer solution in the vicinity of the origin band of the Cy5 $S_1 \rightarrow S_n$ and Cy5.5 $S_1 \rightarrow S_n$ photoinduced absorptions at ~1130 and 1360 nm, respectively, along with fits, rms values, and residuals from the global and target analysis.

The global target analysis on three data set derived a $k_1$ value of $(\frac{1}{0.42 \pm 0.02})$ $ps^{-1}$, which corresponds to a lifetime of ~420 ± 20 fs. The resultant species associated spectra, SAS-1 and SAS-2, are shown in **Figure S20.3**.

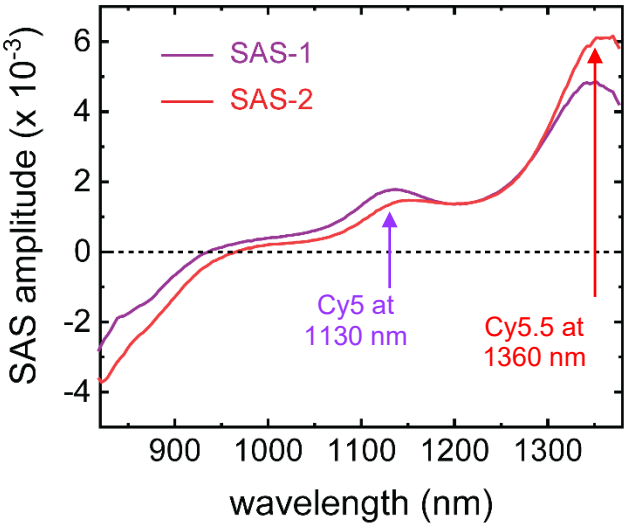


**Figure S20.3.** Species associated spectra, SAS-1 and SAS-2, derived from the global and target analysis of the adjacent dimer solution excited at 650 nm.

Both SAS-1 and SAS-2 exhibit two positive bands at 1130 and 1360 nm and a negative going feature below ~950 nm. The bands at 1130 and 1360 nm were previously assigned to the excited state absorption band of Cy5 and Cy5.5 monomer, respectively, from the near infrared transient absorption measurements, see **Section S19**. **Figure S20.3** shows a clear signature of Cy5 monomer NIR absorption band at 1130 nm that decreases in intensity in SAS-2 while the Cy5.5 monomer NIR absorption band at 1360 increases in SAS-2 is observed in overlaid SAS spectra in **Figure S20.3**. These results are consistent with the interpretation of energy transfer between Cy5 and Cy5.5 in the adjacent heterodimer solution.

**Section S21. Comparison of pump pulse autocorrelation with early-time transient near-infrared absorption kinetics**

In this section, we compare the representative pump pulse autocorrelation (shown in **Figure S3.2.2**) with the early-time transient near-infrared (NIR) absorption kinetics of the Cy5.5 monomer and adjacent heterodimer solutions. The latter data are shown in **Figure 5C** of the main text.

**Figure S21A** plots the pump pulse autocorrelation along with the early-time transient NIR absorption kinetics of the Cy5.5 monomer. The profile of the pump pulse autocorrelation and the early-time transient NIR absorption kinetics of the Cy5.5 monomer exhibit good agreement in the rise time period of the kinetics. Thus, it is possible that the early-time dynamics are convolved with the temporal profile of the pump pulse.

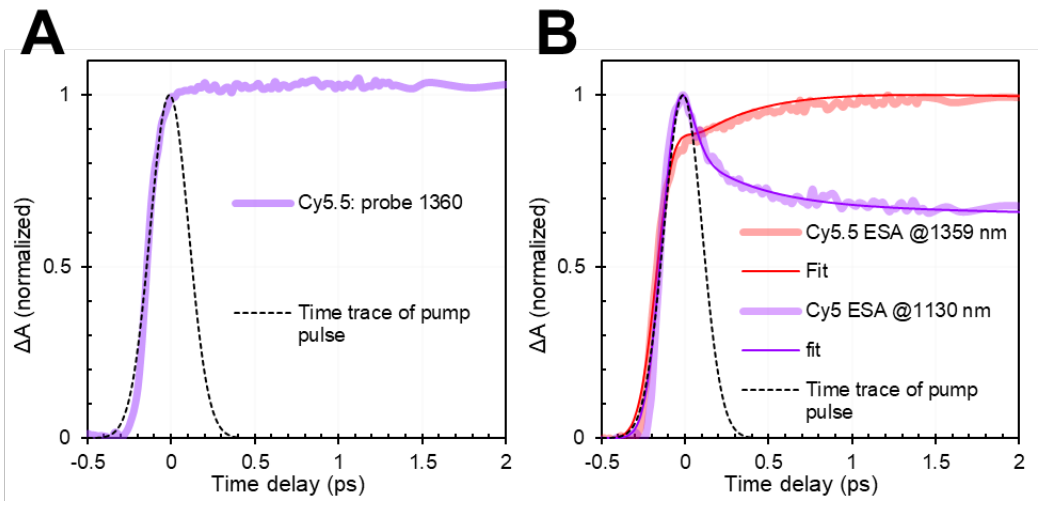


**Figure S21.** Panel **A** shows the overlaid kinetic trace of Cy5.5 ESA band at 1360 nm from the transient NIR absorption measurement of Cy5.5 monomer pumped at 650 nm with the representative pump pulse autocorrelation. Panel **B** shows the overlaid kinetic trace of Cy5 and Cy5.5 ESA bands at 1130 and 1360 nm, respectively, from the transient NIR absorption measurement of adjacent heterodimer solution pumped at 650 nm with the representative pump pulse autocorrelation. The fits from a global target analysis, which yield a time constant of ~420 fs for the conversion of Cy5 ESA to Cy5.5 ESA, are also shown.

**Figure S21B** displays the pump pulse autocorrelation along with the early-time transient NIR kinetics of the transverse heterodimer solution. Again, we find good agreement between the rise of both the pump pulse autocorrelation and the early-time transient NIR kinetics of the transverse heterodimer solution. In this particular dataset, where the excited-state absorption (ESA) signals of Cy5 decay along with the simultaneous growth of the Cy5.5 ESA signals, we also find that the profile of the pump pulse autocorrelation well matches the profile of the rapidly decaying Cy5 ESA signal. This observation indicates that a considerable portion of the dynamics are convolved with the pump pulse. If we take the time constant of ~420 fs derived for the sample dynamics along with the ~230 fs pump pulse duration (see **Section S3**), these values indicate that ~40% of the sample dynamics are convolved with the temporal profile of the pump pulse.

## Section S22. Förster resonance energy transfer explains the energy transfer from Cy5 to Cy5.5 in the adjacent heterodimer

Our results support the interpretation that energy transfer from Cy5 to Cy5.5 in the adjacent heterodimer takes place via Förster resonance energy transfer (FRET).

In FRET, the rate of energy transfer (i.e., $k_{FRET}$) is proportional to the coupling between the donor and acceptor, determined by their orientation and transition dipole moments, and their spectral overlap (**Section S11**).[12,14] The distance between door and acceptor (i.e., $R$) is particularly important in FRET. For example, $k_{FRET}$ can be reliably estimated using a relatively straightforward rate expression in certain limits, i.e., when the dyes are far apart and $R$ is larger than the dye dimensions.[12–14]

Our steady-state and time-resolved measurements provide the first indicator of the distance between the dyes. Our steady-state and time-resolved measurements, which probe the ground- and excited-state electronic structure via $S_0 \rightarrow S_1$, $S_1 \rightarrow S_0$, and $S_1 \rightarrow S_n$ transitions, showed that the dyes undergoing energy transfer exhibit optical properties consistent with monomers. These observations are significant—molecular excitonic theory[11] predicts that the strength of interaction between dyes, i.e., the coupling that changes electronic structure and, as such, optical properties, varies as $R^{-3}$. Thus, from the lack of changes in the optical spectra, which indicates negligible excitonic interactions, we can infer that the dyes are far apart, i.e., $R$ is large.

Next, it would be beneficial to have additional, more quantitative insight on $R$. One way to quantitatively analyze $R$ is from KRM modeling; however, it is not possible to do so in this case because the dyes undergoing energy transfer are not excitonically interacting (**Section S23**). Alternatively, using the expression for $k_{FRET}$ and the measured rate of energy transfer, we can estimate $R$ and evaluate if $R$ is within the limit that we expect for FRET. To make this estimation, we assume that the orientation is isotropic and we take the lifetime of the donor, Cy5, to be 1.7 ns, the Förster radius for Cy5 and Cy5.5 to be 73 Å,[20] and the rate of energy transfer to be $2.4 \times 10^{12}$ $s^{-1}$. $R$ estimated in this manner is ~18.3 Å (**Section S24**). Critically, this value for $R$ is larger than the length of the dyes and is roughly ~20 Å, below which considerable deviations to the estimated $k_{FRET}$ can occur.[14]

Although the estimated $R$ of ~18.3 Å falls slightly below 20 Å, there are a few reasons why. First and foremost, our purpose here is not to accurately determine $R$; rather, it is to provide guidance as to whether the estimated $R$ is within reason of where we expect FRET to still be applicable, which we believe to be the case. The reason the estimated $R$ of ~18.3 Å falls slightly below 20 Å could be explained by a few reasons. First, the estimated value is just at the end limit of where the Forster equation is applicable. Here, small deviations, specifically over-estimations, to $k_{FRET}$ still occur.[14] As such, these small over-estimations would cause estimated $R$ to be an under-estimation of the actual $R$. That is, the actual $R$ may be larger than the $R$ of ~18.3 Å estimated here. An additional, and more likely, factor here is related to dye orientation. The estimation above assumed an isotropic orientation of dyes undergoing energy transfer, which is likely not the case for the Cy5 and Cy5.5 dyes investigated here that are covalently-tethered to DNA. Muñoz-Losa *et al.* showed that significant deviations of $k_{FRET}$, both over- and under-estimations, can occur at interdye separations less than ~50 Å if the dyes are not randomly oriented.[14] Thus, for these

reasons, the actual *R* value could be either smaller or larger than the estimated *R* value of ~18.3 Å, which should be treated as a rough approximation.

In addition to the *R*, we can also estimate the donor and acceptor coupling (*V*) and evaluate the physical reasonability of the estimated value. To do this, we estimated *V* using the following equation:[14]

$$V \approx V_{Coul} \approx V_{dip-dip} = \frac{\kappa|\overrightarrow{\mu_D}||\overrightarrow{\mu_A}|}{4\pi\varepsilon_0 n^2 R_{DA}^3}$$

where $\kappa$ is the orientation factor, $\overrightarrow{\mu_D}$ is the transition dipole moment (TDM) of the donor (D), $\overrightarrow{\mu_A}$ is the TDM of the acceptor (A), *n* is the index of refraction, and $R_{DA}$ is the distance between D and A. In this calculation, we use an orientation factor $\langle\kappa^2\rangle = 2/3$, $\overrightarrow{\mu_D} = \overrightarrow{\mu_A} = 16\ D$, *n* of 1.455 (i.e., the average of the refractive indexes of water [1.332][21] and DNA [1.58][22] at 620 nm), and an $R_{DA}$ value of ~1.8 nm to arrive at a value of *V* of 90 $cm^{-1}$.

The value estimated for *V* of ~90 $cm^{-1}$ is physically reasonable. Considering the value of *V* in terms of excitonic interactions, such a small value would result in negligible changes in the optical properties, i.e., the absorption and CD spectra. For example, a value of *V* of 90 $cm^{-1}$ translates into a shift from ~650 to ~652 nm and ~690 to ~692 nm for Cy5 and Cy5.5 monomer, respectively. While it still may be possible, such small spectral shifts may complicate simulating the optical properties via KRM modeling. Additionally, such spectral shifts are of the order of those expected for changes in solvent environment, i.e., so-called solvatochromic shifts. Thus, it may be difficult to differentiate the changes in optical properties due to excitonic effects from those due to solvatochromic shifts. The absence of changes in the optical properties for dyes separated by this distance is consistent with empirical evidence indicating that when dyes are separated by distances of 2 base pairs (or ~1 nm separation), *V* is small enough such that changes in the optical properties from the monomer are unobservable.[23,24]

The value estimated for V of 90 $cm^{-1}$ is also in the limit of where we expect energy transfer, mediated by FRET, to still be applicable because this level of coupling is less than the homogeneous contribution to the typical absorption linewidth at room temperature. For example, for $V > 100$ $cm^{-1}$ we can expect the constituent dyes to undergo relaxation through a manifold of exciton states; however, for *V* of ~100 $cm^{-1}$ or less the constituent dyes are expected to undergo energy transfer.[25]

With all the observations we conclude that FRET describes the energy transfer from Cy5 and Cy5.5 in adjacent heterodimer.

## Section S23. Difficulty in modeling optical properties to determine interdye separation for Cy5 and Cy5.5 dyes undergoing energy transfer in adjacent heterodimer solution

In principle, modeling of the optical properties can determine the distance between Cy5 and Cy5.5 dyes (i.e., *R*) in the adjacent dimer.

We have found that the adjacent dimer solution is heterogeneous, which is important to determine before undertaking such an analysis. Specifically, the adjacent heterodimer solution consists of a population of dyes that are not excitonically coupled a population of dyes that exhibit excitonic interactions. There are a number of observations supporting this interpretation. For example, the absorption spectrum of the adjacent heterodimer solution is not well-modeled by a one-to-one linear combination of monomer absorption spectra (**Section S10**). While the one-to-one linear combination of monomer absorption spectra models most of the absorption spectrum of the adjacent heterodimer solution, a non-negligible residual is apparent with two prominent features at ~625 and 700 nm. Interestingly, the spectral position of these features is consistent with the spectral position of the negative- and positive-going bands observed in the CD measurement (**Section S6**). Such correlation of observations is consistent with the interpretation that the solution consists of one population of dyes that are not excitonically coupled and another population of dyes are that excitonically interacting. Lastly, the global target analysis of the transient VIS absorption of the adjacent heterodimer solution indicated the presence of a set of rate constants associated with the non-interacting dyes and a third rate constant associated with the interacting dyes (**Section S18**). These results are consistent with the interpretation that the adjacent heterodimer solution is heterogeneous.

The present study focuses on the dynamics of the Cy5 and Cy5.5 dyes in the adjacent heterodimer that do not exhibit excitonic interactions but that undergo energy transfer. In this case, it is not possible to model the optical properties of these dyes, as the optical properties exhibit no changes compared to the monomers. For example, there are an infinite set of orientations possible that could accurately model the optical properties of uncoupled monomers. Thus, it was not possible to obtain *R* for the non-interacting dyes by modeling their optical properties.

**Section S24. Förster equation to estimate the distance between Cy5 and Cy5.5 undergoing energy transfer in adjacent heterodimer**

Here, we apply the Förster equation to estimate the distance between Cy5 and Cy5.5 in the adjacent heterodimer using the measured values. In the limit where the Förster equation is applicable, the rate of energy transfer ($k_{FRET}$) is given by the following equation:[13,26]

$$k_{FRET} = \frac{1}{\tau_D}\left(\frac{R_0}{R}\right)^6$$

For the $R_0$ parameter, we use a value of 73 Å, which was previously determined by Sungchul *et al* for Cy5 and Cy5.5 templated on DNA Holliday junctions.[20] We choose this value because the system studied by Sungchul *et al* is very similar to our study. Using the measured rate of energy transfer of ~420 fs along with the lifetime of Cy5 of ~1.7 ns, we estimate $R$ to be ~18.3 Å.

**Section S25. References**


(1) Cannon, B. L.; Patten, L. K.; Kellis, D. L.; Davis, P. H.; Lee, J.; Graugnard, E.; Yurke, B.; Knowlton, W. B. Large Davydov Splitting and Strong Fluorescence Suppression: An Investigation of Exciton Delocalization in DNA-Templated Holliday Junction Dye Aggregates. *J. Phys. Chem. A* **2018**, *122* (8), 2086–2095. https://doi.org/10.1021/acs.jpca.7b12668.

(2) Breger, J. C.; Susumu, K.; Lasarte-Aragonés, G.; Díaz, S. A.; Brask, J.; Medintz, I. L. Quantum Dot Lipase Biosensor Utilizing a Custom-Synthesized Peptidyl-Ester Substrate. *ACS Sensors* **2020**, *5* (5), 1295–1304. https://doi.org/10.1021/acssensors.9b02291.

(3) Alessi, A.; Salvalaggio, M.; Ruzzon, G. Rhodamine 800 as Reference Substance for Fluorescence Quantum Yield Measurements in Deep Red Emission Range. *J. Lumin.* **2013**, *134*, 385–389. https://doi.org/10.1016/j.jlumin.2012.08.017.

(4) Taniguchi, M.; Lindsey, J. S. Database of Absorption and Fluorescence Spectra of >300 Common Compounds for Use in PhotochemCAD. *Photochem. Photobiol.* **2018**, *94* (2), 290–327. https://doi.org/10.1111/php.12860.

(5) Trebino, R.; DeLong, K. W.; Fittinghoff, D. N.; Sweetser, J. N.; Krumbügel, M. A.; Richman, B. A.; Kane, D. J. Measuring Ultrashort Laser Pulses in the Time-Frequency Domain Using Frequency-Resolved Optical Gating. *Rev. Sci. Instrum.* **1997**, *68* (9), 3277–3295. https://doi.org/10.1063/1.1148286.

(6) Kühn, O.; Renger, T.; May, V. Theory of Exciton-Vibrational Dynamics in Molecular Dimers. *Chem. Phys.* **1996**, *204* (1), 99–114. https://doi.org/10.1016/0301-0104(95)00448-3.

(7) Huff, J. S.; Turner, D. B.; Mass, O. A.; Patten, L. K.; Wilson, C. K.; Roy, S. K.; Barclay, M. S.; Yurke, B.; Knowlton, W. B.; Davis, P. H.; Pensack, R. D. Excited-State Lifetimes of DNA-Templated Cyanine Dimer, Trimer, and Tetramer Aggregates: The Role of Exciton Delocalization, Dye Separation, and DNA Heterogeneity. *J. Phys. Chem. B* **2021**, *125* (36), 10240–10259. https://doi.org/10.1021/acs.jpcb.1c04517.

(8) Mass, O. A.; Wilson, C. K.; Roy, S. K.; Barclay, M. S.; Patten, L. K.; Terpetschnig, E. A.; Lee, J.; Pensack, R. D.; Yurke, B.; Knowlton, W. B. Exciton Delocalization in Indolenine Squaraine Aggregates Templated by DNA Holliday Junction Scaffolds. *J. Phys. Chem. B* **2020**, *124* (43), 9636–9647. https://doi.org/10.1021/acs.jpcb.0c06480.

(9) Barclay, M. S.; Roy, S. K.; Huff, J. S.; Mass, O. A.; Turner, D. B.; Wilson, C. K.; Kellis, D. L.; Terpetschnig, E. A.; Lee, J.; Davis, P. H.; Yurke, B.; Knowlton, W. B.; Pensack, R. D. Rotaxane Rings Promote Oblique Packing and Extended Lifetimes in DNA-Templated Molecular Dye Aggregates. *Commun. Chem.* **2021**, *4* (1), 19. https://doi.org/10.1038/s42004-021-00456-8.

(10) Turro, N. J.; Scaiano, J. C.; Ramamurthy, V. *Modern Molecular Photochemistry of Organic Molecules*; University Science Books: Sausalito, CA, 2010.

(11) Kasha, M.; Rawls, H. R.; Ashraf El-Bayoumi, M. The Exciton Model in Molecular Spectroscopy. *Pure Appl. Chem.* **1965**, *11* (3–4), 371–392. https://doi.org/10.1351/pac196511030371.

(12) Scholes, G. D. Long-Range Resonance Energy Transfer in Molecular Systems. *Annu. Rev. Phys. Chem.* **2003**, *54* (1), 57–87. https://doi.org/10.1146/annurev.physchem.54.011002.103746.

(13) Cunningham, P. D.; Khachatrian, A.; Buckhout-White, S.; Deschamps, J. R.; Goldman, E. R.; Medintz, I. L.; Melinger, J. S. Resonance Energy Transfer in DNA Duplexes Labeled with Localized Dyes. *J. Phys. Chem. B* **2014**, *118* (50), 14555–14565. https://doi.org/10.1021/jp5065006.

(14) Muñoz-Losa, A.; Curutchet, C.; Krueger, B. P.; Hartsell, L. R.; Mennucci, B. Fretting about FRET: Failure of the Ideal Dipole Approximation. *Biophys. J.* **2009**, *96* (12), 4779–4788. https://doi.org/10.1016/j.bpj.2009.03.052.

(15) Rothemund, P. W. K. Folding DNA to Create Nanoscale Shapes and Patterns. *Nature* **2006**, *440* (7082), 297–302. https://doi.org/10.1038/nature04586.

(16) Mirkovic, T.; Ostroumov, E. E.; Anna, J. M.; van Grondelle, R.; Govindjee; Scholes, G. D. Light Absorption and Energy Transfer in the Antenna Complexes of Photosynthetic Organisms. *Chem. Rev.* **2017**, *117* (2), 249–293. https://doi.org/10.1021/acs.chemrev.6b00002.

(17) Huff, J. S.; Davis, P. H.; Christy, A.; Kellis, D. L.; Kandadai, N.; Toa, Z. S. D.; Scholes, G. D.; Yurke, B.; Knowlton, W. B.; Pensack, R. D. DNA-Templated Aggregates of Strongly Coupled Cyanine Dyes: Nonradiative Decay Governs Exciton Lifetimes. *J. Phys. Chem. Lett.* **2019**, *10* (10), 2386–2392. https://doi.org/10.1021/acs.jpclett.9b00404.

(18) Widengren, J.; Schwille, P. Characterization of Photoinduced Isomerization and Back-Isomerization of the Cyanine Dye Cy5 by Fluorescence Correlation Spectroscopy. *J. Phys. Chem. A* **2000**, *104* (27), 6416–6428. https://doi.org/10.1021/jp000059s.

(19) Israels, B.; Albrecht, C. S.; Dang, A.; Barney, M.; von Hippel, P. H.; Marcus, A. H. Submillisecond Conformational Transitions of Short Single-Stranded DNA Lattices by Photon Correlation Single-Molecule Förster Resonance Energy Transfer. *J. Phys. Chem. B* **2021**, *125* (33), 9426–9440. https://doi.org/10.1021/acs.jpcb.1c04119.

(20) Hohng, S.; Joo, C.; Ha, T. Single-Molecule Three-Color FRET. *Biophys. J.* **2004**, *87* (2). https://doi.org/10.1529/biophysj.104.043935.

(21) Hale, G. M.; Querry, M. R. Optical Constants of Water in the 200-Nm to 200-Mm Wavelength Region. *Appl. Opt.* **1973**, *12* (3), 555. https://doi.org/10.1364/AO.12.000555.

(22) Inagaki, T.; Hamm, R. N.; Arakawa, E. T.; Painter, L. R. Optical and Dielectric Properties of DNA in the Extreme Ultraviolet. *J. Chem. Phys.* **1974**, *61* (10), 4246–4250. https://doi.org/10.1063/1.1681724.

(23) Cannon, B. L.; Kellis, D. L.; Patten, L. K.; Davis, P. H.; Lee, J.; Graugnard, E.; Yurke, B.;

Knowlton, W. B. Coherent Exciton Delocalization in a Two-State DNA-Templated Dye Aggregate System. *J. Phys. Chem. A* **2017**, *121* (37), 6905–6916. https://doi.org/10.1021/acs.jpca.7b04344.

(24) Cunningham, P. D.; Kim, Y. C.; Díaz, S. A.; Buckhout-White, S.; Mathur, D.; Medintz, I. L.; Melinger, J. S. Optical Properties of Vibronically Coupled Cy3 Dimers on DNA Scaffolds. *J. Phys. Chem. B* **2018**, *122* (19), 5020–5029. https://doi.org/10.1021/acs.jpcb.8b02134.

(25) Scholes, G. D.; Mirkovic, T.; Turner, D. B.; Fassioli, F.; Buchleitner, A. Solar Light Harvesting by Energy Transfer: From Ecology to Coherence. *Energy Environ. Sci.* **2012**, *5* (11), 9374. https://doi.org/10.1039/c2ee23013e.

(26) Clegg, R. M. [18] Fluorescence Resonance Energy Transfer and Nucleic Acids; 1992; pp 353–388. https://doi.org/10.1016/0076-6879(92)11020-J.